MASSACHUSETTS INSTITUTE OF TECHNOLOGY
ARTIFICIAL INTELLIGENCE LABORATORY

A. I. Memo No. 648 19 August 1981

A Lightness Scale from Image Intensity Distributions

W. A. Richards

Abstract

A lightness scale is derived from a theoretical estimate of the probability distribution of image intensities for natural scenes. The derived image intensity distribution considers three factors: reflectance, surface orientation and illumination, and surface texture (or roughness). The convolution of the effects of these three factors yields the theoretical probability distribution of image intensities. A useful lightness scale should be the integral of this probability density function, for then equal intervals along the scale are equally probable and carry equal information. The result is a scale similar to that used in photography, or by the nervous system as its transfer function.

Acknowledgement. This report describes research done at the Department of Psychology and the Artificial Intelligence Laboratory of the Massachusetts Institute of Technology. Support for this work is provided in part by the Advanced Research Projects Agency of the Department of Defense under Office of Naval Research contract N00014-80-C-0505 and in part by NSF and AFOSR under a combined grant for studies in Natural Computation, grant 79-23110-MCS. Technical assistance was provided by Carol Papineau. The critical comments of Eric Grimson in particular and others in the vision group at MIT were greatly appreciated.

1.0 Introduction

A lightness scale is a rule for assigning numbers to the possible range of light intensities encountered in a natural world. Clearly the exact form of the scale will depend upon the objectives of the sensing device. Because the possible range of intensities is quite large (10^8), most practical lightness scales involve compressive transformations to limit the output (scale) range to 10^2 or so. Common examples are the transfer functions used in photography, TV, or by the human eye.

One striking feature of these examples is that the scales characterized by the transfer functions are remarkably similar, suggesting that each scale has roughly the same objective. Considering that both TV and photography are aimed to please the human viewer, the root of the similarity has generally been taken to be the transfer function of the human eye. Consequently, most theories of lightness scales have begun by considering the constraints the visual mechanism imposes upon the stimulus-response relation (Judd and Wysecki, 1975). For example, if the observed threshold intensity change is proportional to intensity (Weber's Law), and one assumes that any just-noticeable-intensity change corresponds to a fixed sensory increment, then Fechner (1860) argues that the resultant lightness scale will be the logarithm of intensity. Stevens (1961), on the other hand, disputes this assumption of a constant sensory increment regardless of sensation magnitude, and proposes a power law for a lightness scale. Other assumptions about the mechanism have led to many other proposals (Van de Grind, et al, 1971; Treisman, 1966; MacKay, 1963).

Yet in spite of the many different proposals, the resultant lightness scales are still remarkably similar over any 1000-fold range of intensities. Clearly, all of these competing assumptions cannot be correct simultaneously in the same mechanism. Rather, they illustrate that there are many different ways of achieving essentially the same lightness scale (Resnikoff, 1975). But why is the end result always the same? Clearly, there must be some constraining influence independent of the mechanism that is the major factor in determining the useful form of a lightness scale. This study proposes that this factor is the probability distribution of intensities in the world as seen by *any* visual system, whether it be an eye or a camera. The mode of processing is irrelevant. What matters most is the need to respond to the distributions of intensities in the world in an efficient manner, regardless of the exact nature of the visual device (Marr, 1982). This reasoning thus leads to the following simple starting point for a lightness scale:

Proposal: *A useful lightness scale will be one that, on average, will sample the expected image intensities in such a manner to optimize the encoding of the available intensity information.*

Thus, in contrast with the previous approaches, the present derivation simply asks what lightness scale would optimize the information content of each intensity sample regardless of the nature of the sensory mechanism. In any given scene, the distribution of intensity values will generally be quite non-uniform, with intermediate "gray" values being the most common and "blacks" of zero intensity and "whites" of great intensity occurring rarely. It then clearly makes sense to sample the middle grays more carefully and the extremes less so. Such considerations yield a lightness scale where the principal constraints upon the scale will be the external properties of the world, rather than the internal properties of the visual mechanism.

2.0 Background: The Image Intensity Equation

To determine an optimal lightness scale first requires determining the probability distribution of image intensities falling upon a retina. Such distributions have not previously been calculated for the factors of interest here. Although many texts on geometrical optics describe how light is reflected off surfaces (Keitz, 1971), they do not address the problem of how frequently one encounters any particular image intensity value. Without knowledge of this latter *probability* distribution, we have no way of specifying a scale (or transfer function) that will sample the image intensities in an optimal manner. To solve for the expected probability distribution of intensities in the image, the image intensity associated with any small surface patch must be calculated, and then the areal projection of this patch on the retina must be integrated with all patches of similar image intensities. This total for each image intensity value, relative to the total retinal area under consideration, will determine the probability of encountering that particular image intensity value.

To proceed, we consider first the factors that affect the image intensity corresponding to any small patch of surface as projected onto a retina. These include primarily the strength and spectral composition of the illuminant, its angular position relative to the viewer, the orientation and reflectance of the viewed surface, its reflectivity function including textural, spectral and specular factors (Horn and Sjoberg, 1979). These many factors combine together multiplicatively to produce the image intensity $I(\lambda)$ associated with the patch of surface of reflectance (albedo) $\rho(\lambda)$, illuminated by a source of strength $E(\lambda)$:

$$I(\lambda) = \rho(\lambda)E(\lambda)(\mathbf{NL})R(\sigma,\theta) \tag{1}$$

where the term $(\mathbf{N} \cdot \mathbf{L})$ reflects the orientation of the surface normal $\mathbf{N}$ and illuminant direction $\mathbf{L}$ relative to the viewer (see Fig. 4) and where $R(\sigma,\theta)$ is the reflectivity function that characterizes the textural and specular properties of the surface. (Although the image intensity equation (1) is a function of wavelength λ, this dependence will be ignored in subsequent derivations.)

To simplify the recovery of scene properties from image information, it is desirable to remove the effects of the overall illuminant strength by setting $E(\lambda) = 1$. This normalization, together with the multiplicative behavior of the remaining contributions to image intensity, generally leads to the examination of intensity ratios (Helmholtz, 1910;Land and McCann, 1971). A useful lightness scale will therefore be a ratio scale.

In sum, three factors are the primary contributors to achromatic image intensities: reflectance, ρ; surface orientation and illuminant position $(\mathbf{N} \cdot \mathbf{L})$; and the reflectivity properties of the surface, $R(\sigma,\theta)$, especially its textural properties. For each of these factors, probability density functions can be determined by calculating the relative retinal area associated with any given image intensity. Since the three factors are independent, the desired probability distribution of retinal image intensities will be the joint probability density function for all these factors, calculated by convolving the three independent density functions.

The first objective will be to show that this resultant probability density function is roughly log-normal and thus can be specified by two numbers—a mean and a standard deviation. The second objective will be to show how this log-normal distribution of image intensities constrains the shape of an ideal lightness scale.

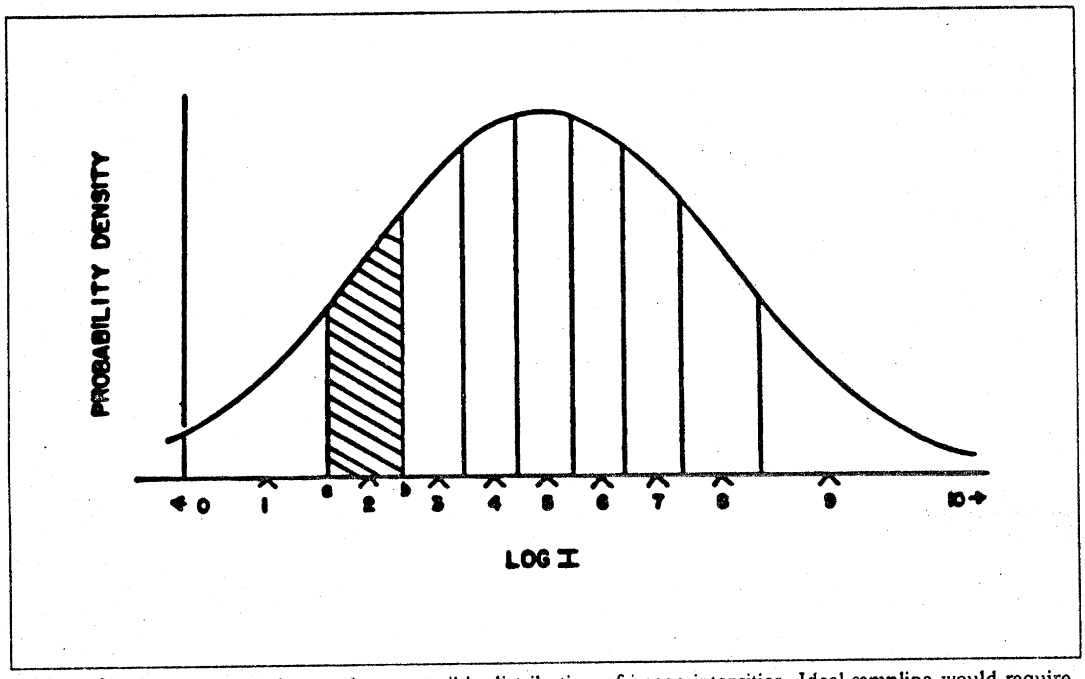

Figure 1. The envelope characterizes a possible distribution of image intensities. Ideal sampling would require the measurements be taken such that each interval has an equal area under the curve and hence is equally likely.

3.0 The Normal Log Approximation

Lemma 1. The most probable (mean) image intensity will be the product of the mean intensities of the separate probability distributions of the N factors affecting image intensity and the variance of the resultant joint probability distribution plotted on a $logI$ axis will be the sum of the squares of the N independent variances (also measured in terms of $logI$).

The above lemma follows straightforwardly from the Central Limit Theorem, provided that each density function is convolved on a $LogI$ continuum (Bracewell, 1978). Note that the convolutions cannot be performed on a linear continuum on I because intensities multiply, rather than add as required in the convolution integral. The log transformation thus permits the addition of the pairs of variables as each convolution is performed. As N increases without limit, the distribution will therefore approach a Gaussian on a $logI$ axis, which is the log-normal function. However, even for small N, excellent approximations to the log-normal function can be achieved, provided that each individual probability distribution has finite (positive) area, mean, variance and third moments. (Our derived distributions will satisfy these properties.)

Because the mean image intensity is somewhat arbitrary, depending upon the normalization procedure, the problem of defining a lightness scale based upon multiple, independent factors reduces to finding the standard deviation of the Gaussian distribution defined on a $logI$ axis. Our procedure, then, will be to calculate the variances of the image intensity probability distributions arising from three factors: reflectance, surface orientation and lighting direction, and textural shadow and to use the sum of these variances (on $logI$) to define a Gaussian approximation to the distribution of image intensities. This probability distribution, in turn can be used to construct a useful lightness scale. Prior to estimating the three variances, the general strategy for creating a lightness scale will be considered.

4.0 An Ideal Lightness Scale

Before embarking on a more exact probability density function for image intensities, it is helpful to illustrate first why such a density function may be used to create a useful lightness scale. Assume that the form of this ideal density function is Gaussian on a $logI$ continuum centered about some mean value I_{avg}. Given this *a priori* Gaussian distribution of (log) image intensities, the problem is to decide where on the (log) intensity continuum the sample measurements be taken, and specifically at what intervals. Three constraints will be imposed:

1. Although each measurement will be centered at fixed positions along the $logI$ continuum, the value measured will be the total density within a window where the window sizes are such that together the total range of intensities is spanned.

2. Each measurement will be independent of another. Thus the "windows" will not overlap.

3. The total amount of information should be maximized (over time).

The first two constraints merely define the nature of the "channels" that sample the range of intensities. Referring to Fig. 1, the "carets" indicate the "centers" of nine hypothetical "channels" that sample the $logI$ intensity continuum. The width of the "channels" is indicated by the vertical bars placed under the Gaussian envelope.

Let p_2 be the probability of an image intensity falling into the 2nd measurement "channel". Then the expected value of p_2 is

$$p_2 = \frac{1}{\sqrt{2\pi}} \int_a^b \quad exp - \frac{1}{2}(logI/I_{avg})^2 d(logI) \tag{2}$$

which is the cross-hatched area in Fig. 1. The third constraint that the total measurement information H be maximized is equivalent to maximizing

$$H = \sum_i^N -p_i log \quad p_i \tag{3}$$

where p_i is defined as in (2). To maximize H, it can be shown that $p_i = p_j = \frac{1}{N}$, where N is the number of measurement samples or "channels" (Brillouin, 1962). Thus, the third constraint will be satisfied if the area between the vertical bars in Fig. 1 are equal.

If image intensities are distributed normally, therefore, a reasonable choice for a lightness scale will be to choose intervals that yield equal areas under the Gaussian envelope. For a ten-point scale, the first $logI$ value will be located at a log I/I_{avg} value of -1.22, which would correspond to an I/I_{avg} ratio of 3.9 for a natural log base. Continuing this procedure, we obtain the lightness scale function depicted in Fig. 2 (Gaussian assumption). The locus is a straight line because log-normal axes have been chosen. (This relation between subjective scales and information-rich variables has been known for some time (Zipf, 1949; Richards, 1967).

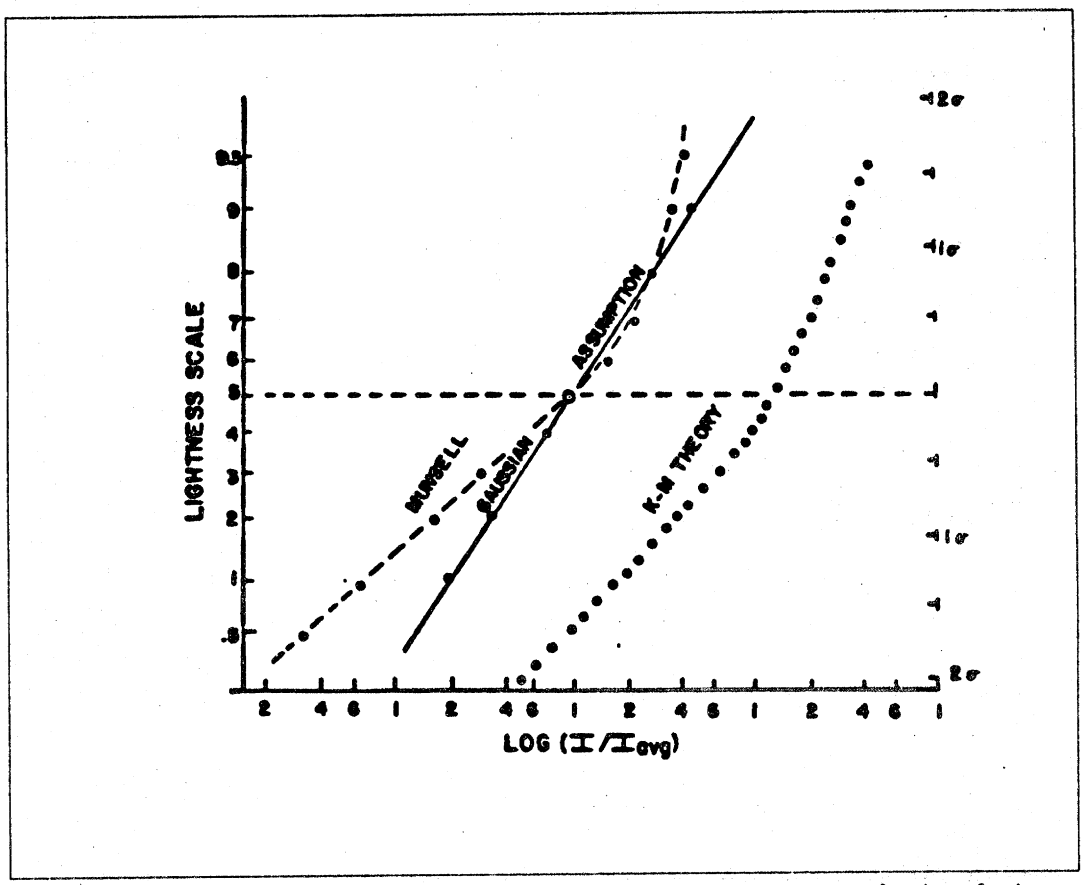

Figure 2. Lightness scales constructed by integration of various theoretical density functions for image intensities. The ordinate is in units of standard deviation, and thus a Gaussian probability distribution of (log) image intensities, such as in Fig. 1, will yield a straight line. A more plausible basis for a lightness scale is the Kubelka-Munk theory of reflectance, which yields the curve labelled "K-M Theory". This result begins to approximate a common scale (Munsell) shown at left.

5.0 Estimating three independent density functions

As previously discussed, the Central Limit Theorem assures us that the combination of multiplicative factors that contribute to image intensities will tend to produce a Gaussian probability density function on a *logI* continuum, as more and more factors are considered. However, although the approximate form of the final image-intensity density function is known, two parameters remain to define the shape and position of the Gaussian: its mean and standard deviation. These unknowns set the horizontal position and slope of the straight-line lightness scale in Figure 2. Since by appropriate normalization, the mean can be set to the midpoint of the scale, as it is in Figure 2, the standard deviation of the Gaussian remains the principle single unknown. How can this unknown be found?

Our procedure will be to estimate the image intensity distribution for each of the three major factors in the image-intensity equation (1). This will result in three separate probability density functions (*pdf*), one for reflectance, another for surface orientation and illumination, and a third for surface roughness or texture. The final distribution of image intensities will then be the convolution of these three independent density functions. The final lightness scale will be the integral of this joint probability distribution function, suitably normalized.

If each of the individual density functions were approximately Gaussian, then the final joint-density function could be obtained simply by adding together the standard-deviations (on *logI*) of the component functions. However, because each factor, such as reflectance, cannot exceed 1, the observed individual density functions will not be Gaussian. Furthermore, because of this assumption, when the individual density functions are integrated, they will depart considerably from the straight-line "ideal" lightness scale, as illustrated by the two broken curves in Figure 2. A "practical" lightness scale will therefore not be a straight-line on a log-normal graph. To find its shape, numerical convolutions of the three component density functions must thus be performed, once each function has been estimated.[1]

5.1 Estimating the Density Function for Reflectance

As we examine the properties of materials in the world about us, we note that their achromatic reflectances cover the range from black to white, with these two extremes corresponding to completely absorbing materials (such as carbon black) to completely non-absorbing or light scattering materials (such as snow or pure cellulose). It is not unnatural to view the intermediate grays as some mixture of these two extremes, because absorption and scatter are the two primary properties that determine the reflectance (albedo) of a material. For many natural materials, such as wood, grass or even silica-based minerals, most of the scattering of light comes from the "white" substrate to which the added pigment (or metallic impurities) provides most of the absorption. Many natural materials then may be considered to be made up of two types of particles–a pigmented particle that is responsible for the absorption, and a non-pigmented "white" particle that comprises the substrate and causes most of the scatter. For such materials, the reflectance will depend upon the relative amount of pigmented particles in the white substrate.

To estimate the distribution of image intensities arising solely from reflectance changes, we therefore will follow Judd and Wysecki (1975) and consider an "ideal" achromatic material as one made up of various portions of ideally absorbing pigment and an ideally scattering "white" substrate. By using the Kubelka-Munk theory of reflectance, we can now relate the absorbing and scattering properties of such a material to its reflectance. With a simple assumption about the distribution of pigment in materials, the desired probability density function for reflectance can then be obtained.

Appendix I shows that for an opaque surface made up of fine particles in a clear medium, the limiting reflectance of the surface can be described by the following relations between the pigment concentration, C, and the absorbing power a, of the material. (The parameter a is the ratio of the absorption coefficient of the ideal pigment to the scattering coefficient of the ideal substrate.)

$$\rho = 1 + \frac{Ca}{(1-C)} - \frac{Ca}{(1-C)}\left\{1 + \frac{2(1-C)}{Ca}\right\}^{\frac{1}{2}} \tag{4}$$

Since the value of a will be fixed and is determined simply by measurements of the coefficients of highly scattering and highly absorbing materials, the principle unknown in equation (4) is the value of

[1] All calculations and convolutions were performed on an Apple II computer.

the pigment concentration, C. However, C is itself a distribution function. To find the distribution of reflectance ρ we must therefore have some knowledge of the distribution of pigment in materials. Specifically, we need a probability density function (*pdf*) for the pigment concentration, C. Once the $pdf(C)$ is known, we can apply Bayes Rule to determine the density function for reflectance, ρ:

$$pdf(\rho) = pdf(C) \cdot \frac{d(C)}{d(\rho)} \tag{5}$$

The simplest assumption about the distribution of pigment concentration is that it increases monotonically to some asymptotic level, following a growth curve. This is most certainly the case for many natural materials such as foliage, grass and trees, which occupy the largest portion of our reflecting environment. Recognizing that the time for growth is much shorter than the adult lifespan of a material, the density function for pigment concentration can be approximated by a power relation:

$$pdf(C) = C^{\beta} \tag{6}$$

where the exponent β lies between 0 and 1 and C is defined over the same range. With this rather weak assumption, Appendix I shows that the probability density function for reflectance will be

$$pdf(\rho) = \frac{2\alpha^{\beta+1}(1-\rho)^{2\beta}(1-\rho^2)}{[\alpha + (2-2\alpha)\rho + \rho^2]^{\beta+2}} \tag{7}$$

where α is a material constant describing the ratio of the scatter to absorption coefficients. This function is plotted as the smooth curve in Figure 3 for $\alpha = \frac{1}{2}$ and $\beta = \frac{1}{2}$. The histogram is an empirical distribution of the reflectances of natural materials taken from a compilation by Krinov (1971). The mean of both distributions is about .15.

The choice of the two parameters β and α can be justified independently of the good fit to Krinov's measurements. First, the exponent for β should be considerably less that 1, in order that the "mature" concentration of the adult material be the most common. However, β cannot be as small as zero, otherwise the growth processes would not be represented. Given no other constraints, a β value of $\frac{1}{2}$ is the best compromise between these two undesirable extremes. (In practice, any β value ranging from $\frac{1}{4}$ to $\frac{3}{4}$ will not significantly alter the lightness scale result, as shown in Appendix I.)

The choice of the scatter to absorption coefficient, α, is dictated simply by measurements of coefficients of highly scattering and absorbing materials, such as white and black (or dark gray) paints. From Davidson and Hemmendinger (1966), a maximally practical scatter coefficient is about 10, whereas the absorption coefficient of a black pigment will be about 100. A dark gray pigment, however, will have an absorption coefficient of about 10 to 20. Considering that the spectral absorption band of most natural pigments is not flat like carbon black, but rather confined to a portion of the spectrum, their coefficient will be in the range 10 — 20. Although this coefficient is lower than that for carbon black, it is important to note that a material consisting entirely of an absorbing pigment with no scatter at all will appear black, regardless of the absorption coefficient of the pigment. The effect of the absorption coefficient is merely to control the rate at which any increase in pigment concentration

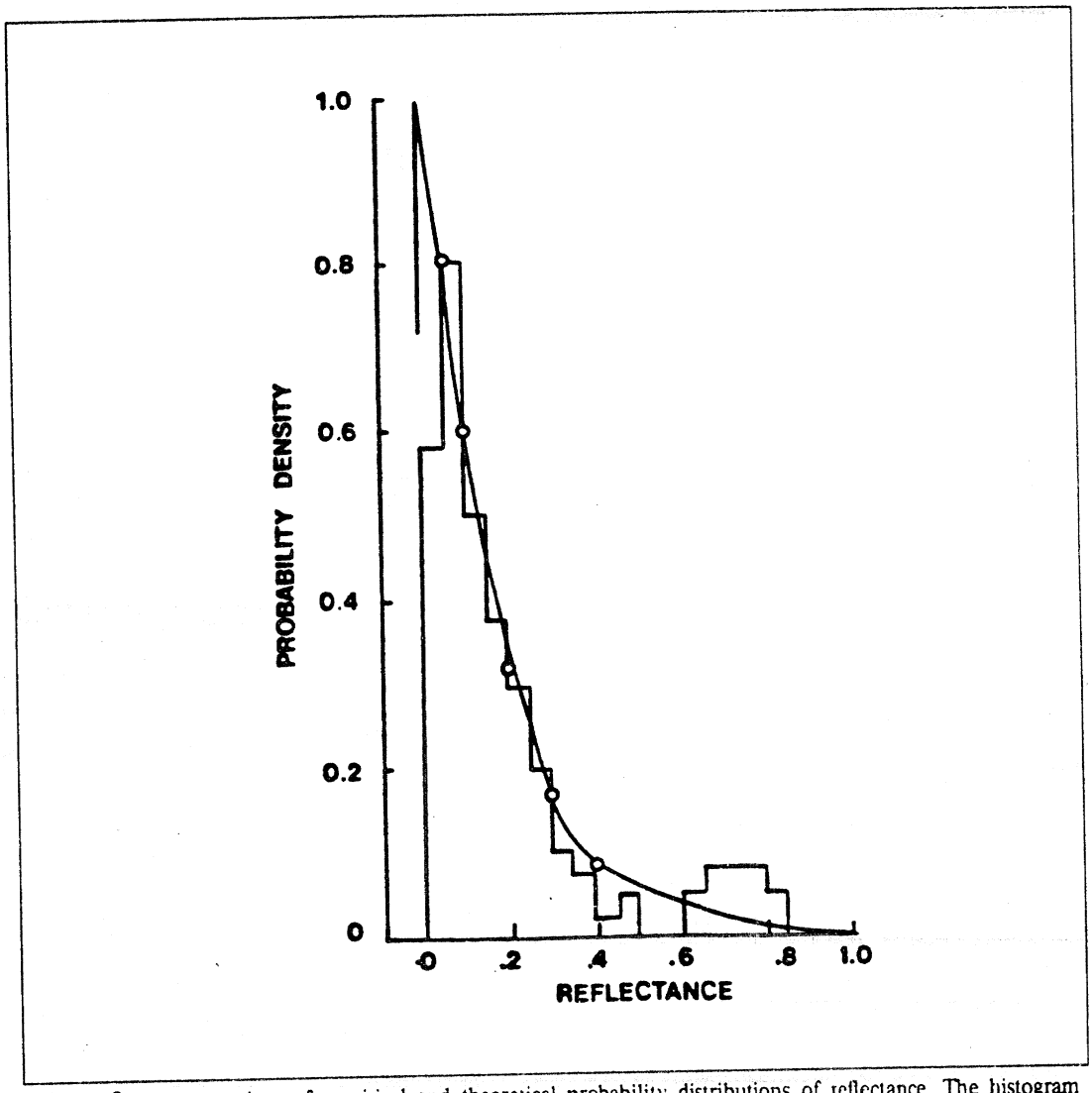

Figure 3. A comparison of empirical and theoretical probability distributions of reflectance. The histogram is an empirical distribution of the reflectances of natural materials taken from a compilation by Krinov (1971). The smooth curve is a theoretical probability distribution based upon an extension of the Kubelka-Munk theory.

causes a reduction in reflectance. With the scatter coefficient of the "white" substrate taken as 10 and the absorption coefficient of the pigment as 10 to 20, the parameter α will range from 0.5 to 1. The former value was chosen to give a distribution of reflectances close to Krinov's.

The function described by equation (7) and illustrated in Figure 3 for $\alpha, \beta = \frac{1}{2}$ is our estimate of the expected probability distribution of reflectance. On a *logI* scale, its variance is approximately 3.3^2 or 10. As shown in Appendix I, this value is relatively insensitive to the choices for α and β. When integrated, the reflectance-density function yields the curve labelled "K-M Theory" in Figure 2. Because of the upper bound of 1 placed upon reflectances, this curve rises rapidly above its mean value, and more closely resembles the most common lightness scale–the Munsell Scale. However, for natural scenes, two other image-intensity factors must still be evaluated before a final practical

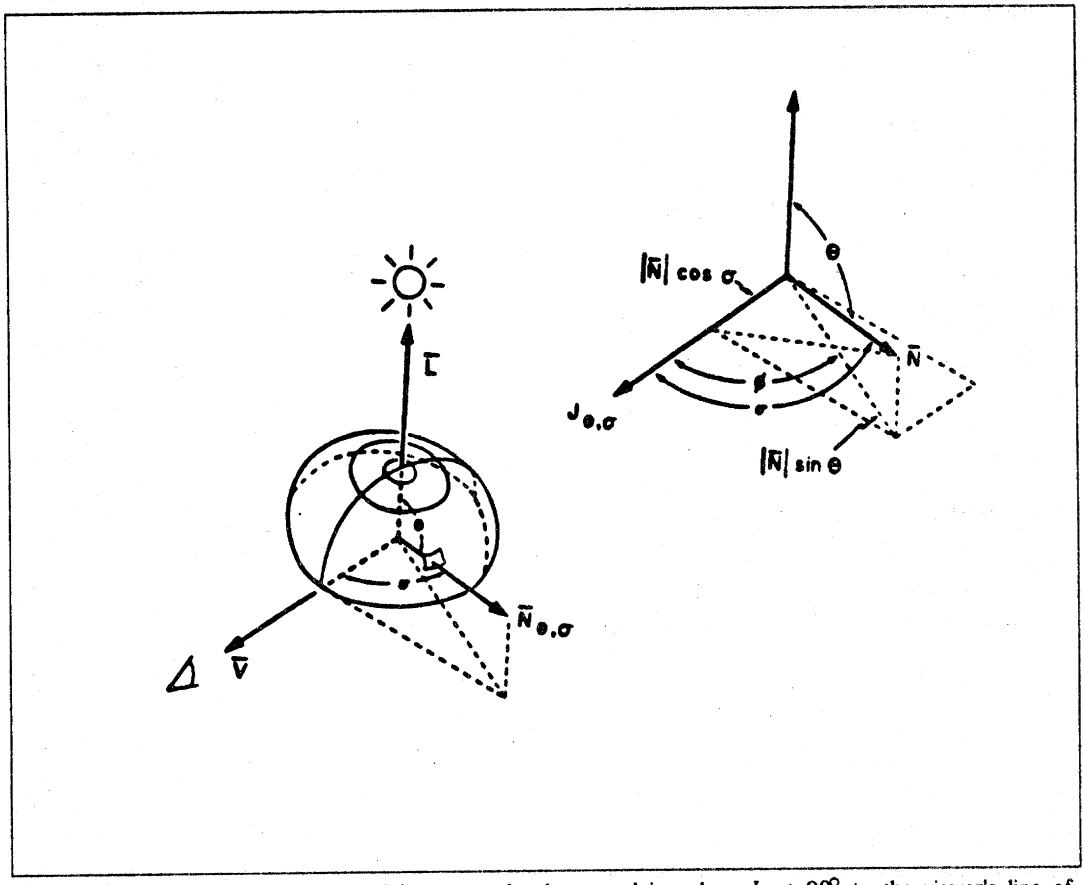

Figure 4. A hemisphere illuminated by an overhead source lying along L at 90° to the viewer's line of regard V. As before, N is the surface normal and J is the flux emitted in the viewer's direction. The inset defines the slant angle, σ. Orthographic projections and Lambertian surfaces are assumed.

lightness scale can be constructed.

5.2 Surface orientation and lighting

A factor second to reflectance in producing image intensity variations is surface orientation relative to the illuminant direction. These effects are characterized by the $\mathbf{N} \cdot \mathbf{L}$ term in equation (1), where $\mathbf{N}$ is the (vector) orientation of the surface normal relative to the viewing direction $\mathbf{V}$, and $\mathbf{L}$ is the illuminant direction. (See Figure 4.) When sunlight strikes a uniformly reflecting sphere, the surface perpendicular to the rays is intensely lit, whereas the parallel edge or the back side is dark or only dimly illuminated by diffuse light. How do these illumination effects alter the expected lightness scale? Specifically, we wish to calculate the probability density function for surface effects so that this probability distribution may be convolved with the pdf for reflectance alone. Two cases of illumination will be considered: extended and direct overhead.

5.2.1 Extended Illumination

When the sky is completely overcast, as object is illuminated almost equally from all directions. Reflectance and surface orientation relative to the viewer then become the two major factors in determining image intensity. For a surface of constant reflectance, image intensity will be a function solely of surface orientation[2].

A major class of natural surfaces are those that act like a perfect diffuser. (These are called Lambertian surfaces.) For such surfaces, it is well known that the combined effects of surface orientation and illuminant direction are exactly cancelled by the foreshortening of the surface patch relative to the viewing angle (Wysecki and Stiles 1967). The effective image intensity I per unit area is thus simply proportional to the incident flux on the surface patch of interest. But if the illumination is extended, then the total incident flux is constant everywhere on the surface and the distribution of image intensities arising solely from surface orientation will be a spike at 1.

Thus, for Lambertian surfaces seen under extended illumination, surface orientation and lighting will have no effect on the expected probability distribution of image intensities.

5.2.2 Overhead Illumination

A second natural lighting condition is when the sun directly illuminates surfaces from overhead as at "high noon". Figure 4 depicts the relations between the viewer **V**, the illuminant direction, **L**, and the normal vector to the surface, **N**. What is the expected probability distribution of image intensities in this case?

To simplify the analysis, the following assumptions will be made:

i) the view is orthographic–i.e. there is a parallel projection onto the image;

ii) there is a uniform distribution for the slant of all surfaces relative to the viewer. The view of sphere can thus be taken to represent this distribution;

iii) the surfaces are Lambertian;

iv)there is a 90° angle between the viewer and the source (i.e., $(\mathbf{V} \cdot \mathbf{L}) = 0$).

Referring to Figure 4, we see that the horizontal circles about the illuminant axis **L** will correspond to loci of constant slant to the source, and hence reflect equal flux, whereas vertical circles (not shown) about the viewer's axis **V** will have equal foreshortening. The net image intensity will be a combination of these two factors. The problem is to determine the loci of constant image intensity as seen by the viewer and to measure their relative sizes, thereby determining the weights that should be given to each image intensity.

The derivation of this density function is given in Appendix II. Surprisingly, the result is quite simple:

$$pdf(I) = [1 - I^2] \tag{8}$$

[2]The underneath surface of an object may be illuminated to a lesser degree than the top, because the diffuse reflectance of the ground is less than that of the sky. Such differences will be ignored here.

where I represents the intensities arising solely from the variations in the $[\mathbf{N} \cdot \mathbf{L}]$ factor in equation (1). This density function is shown in Figure 5 as the solid curve labelled $E = 0$. (The spike at $E = 1$ is the previous case where all the illumination is extended.)

5.2.3 Overhead plus diffuse illumination

In the more common case, diffuse illumination of surfaces will also be present. A portion of this diffuse illumination may come from the sky, and a second portion may be reflected off the array of surrounding surfaces. For simplification, we will assume that all of the diffuse contribution to image intensities is reflected off surrounding surfaces. In this case, as shown in Appendix III, on the average, 20% of the total illumination will come from diffuse reflection. This diffuse light contribution can now be included with the direct source illumination to calculate a new density function for overhead plus diffuse illumination. The dotted curve labelled $E = .2$ in Figure 5 shows the form of this function, which will be the one chosen to represent the contribution of the $(\mathbf{N} \cdot \mathbf{L})$ factor in the image intensity equation (1). The variance of this function is approximately 3 (on a $logI$), with a mean value of 0.4.

5.3 Textured surfaces and shading

The third factor affecting the distribution of image intensities is the reflectivity function $R(\theta, \sigma)$. Generally this term in the image-intensity equation is used to describe the specular properties of the surface, which depend dramatically upon the surface orientation relative to the viewer and illuminant direction. Hence the angular parameters θ, σ (Horn and Sjoberg, 1979). However, because of its highly directional nature (Torrance and Sparrow, 1967), specularities represent only a very small contribution to the total distribution of image intensities. A much more important factor is the structure of the surface itself, namely its roughness or textural quality.

Surface texture generally arises from three-dimensional "elements" that are the constituents of the underlying two-dimensional surface seen at a much larger scale. Such "elements" may be blades of grass, or leaves at many orientations, or the pebbles on a beach. Because the elements are three-dimensional, they produce self-shading and shadows. In order to estimate the image intensity density function for surface texture, it is necessary to model the effects of these small, three-dimensional surface elements. Two such models will be considered. The first is a surface texture created by distributing cylinderical "matchsticks" on a planar sheet (simulating a "lawn"); the second is the texture created by strewing spheres on a flat surface. This latter model texture is particularly useful because it captures the essential properties of many natural surfaces. For example, the resultant distribution of intensities is a very good approximation to that actually measured for shrubbery. Our explanation for this similarity is that within a sufficiently large region of the shrub (relative to leaf size), all orientations of the leaf are equally likely and hence, each leaf can be mapped onto a different portion of a model sphere that represents that portion of the shrub. The fact that most shrubs (or trees) have

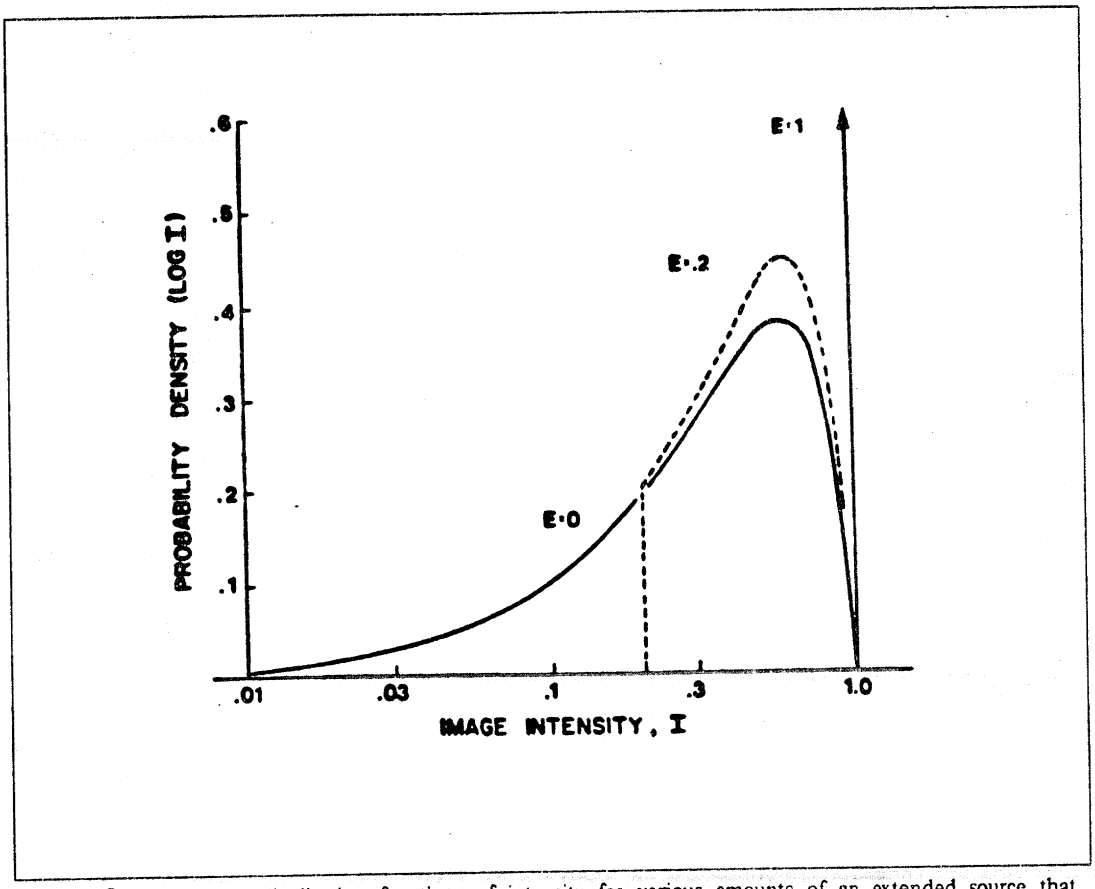

Figure 5. Probability distribution functions of intensity for various amounts of an extended source that, together with an overhead point source, illuminate a uniform distribution of surface orientations. Point source alone: $E = 0$; 20% extended illumination; $E = .2$; extended illumination alone: $E = 1$.

a round shape will further strengthen the success of the model when the image intensities are taken from the entire object.

Figure 6 summarizes the probability density function for image-intensity arising from textured surfaces that can be modelled either by spheres or cylinders lying on a planar substrate of the same material. (Refer to Appedix III for derivations.) Both types of density functions are very similar, with a sharp peak at the lower image intensities corresponding to the dark cracks or shadows between the textural elements. (See Fig. C5.) The position and magnitude of this "spike" will, of course, depend upon the density of the textural elements. The parameter S in Fig. 6 shows how the space between the elements alters the resultant probability density function.

For the case of a planar surface textured by abutting spheres of identical size and reflectance, with uniform illumination, the "gap" between the spheres corresponds to the shadowed region and contributes to 1/8th of the total image intensity distribution. (This is the "spike" in Appendix Figure B2.) Thus, the major contribution to the density function for "pebbled" textured surfaces comes from the surface of the spherical elements. As shown in Appendix III, this portion of the probability density function (pdf) may be approximated by the rather simple formula:

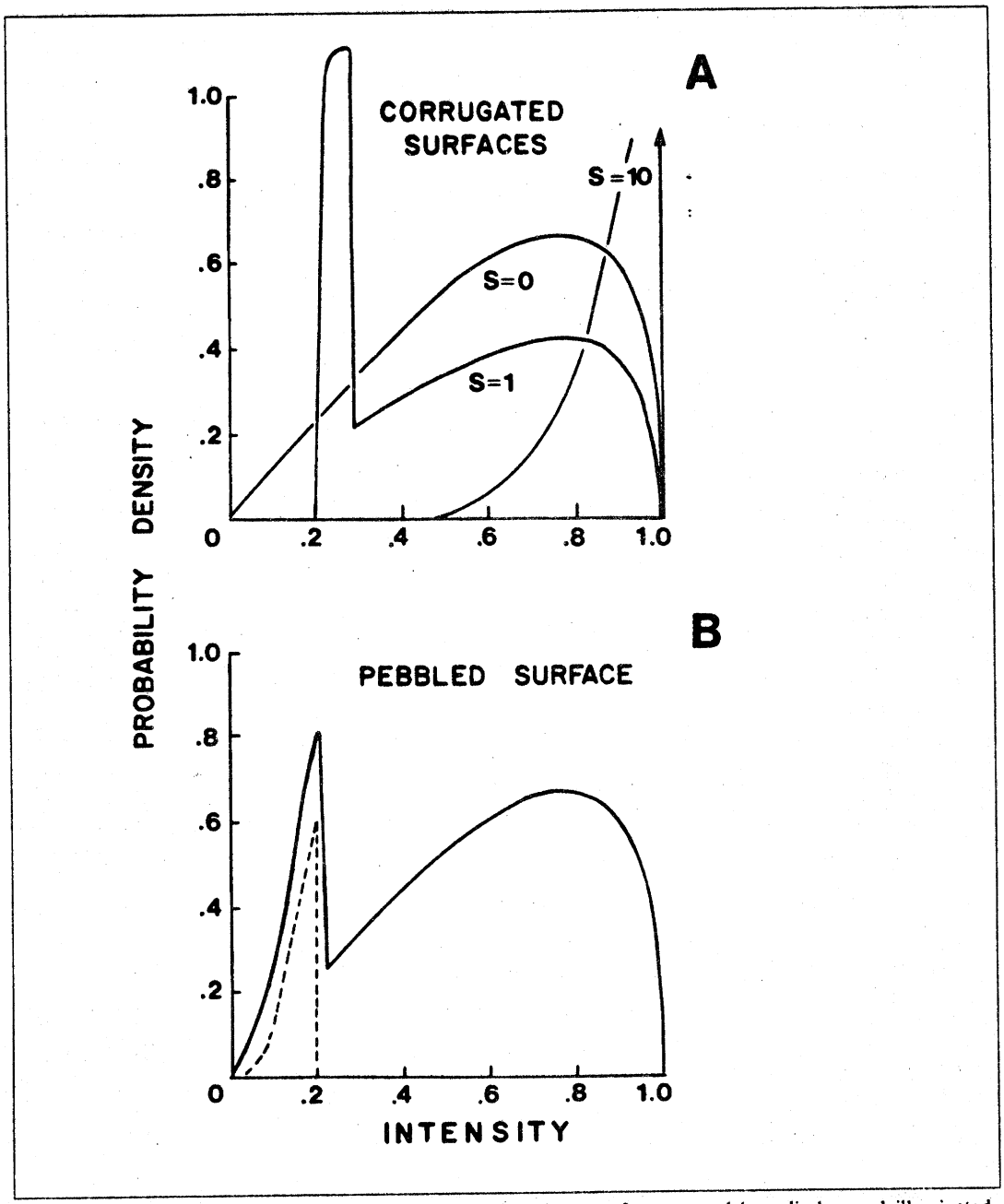

Figure 6. (A) Probability distribution of intensity values for a surface textured by cylinders and illuminated by a hemispheric source, such as the sky. Each curve is for a different separation of the cylinders, with the gap (S) measured in radius units. (B) Distribution of intensity values for a surface "pebbled" by abutting spheres, illuminated by an extended overhead source such as the sky. Refer to Appendix III, Fig. C5 for a comparison of the model with an image intensity distribution taken from a natural object.

$$pdf(I) = I^2(1 - I^2)^{\frac{1}{2}} \tag{9}$$

This function is plotted as the curve T_1 on a $logI$ axis in Figure 7. The dashed curve labeled T_2 is the contribution from the gap, and C is the combined result. The mean of this combined texture density

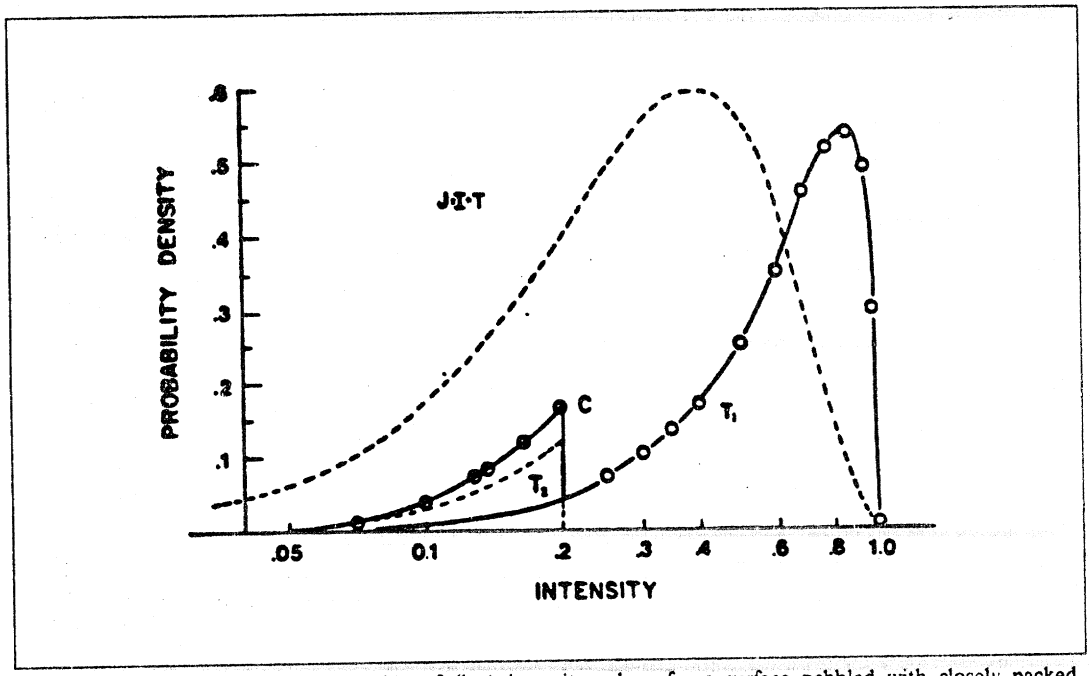

Figure 7. The probability distribution of (log) intensity values for a surface pebbled with closely packed spheres (T). The components T_1 and T_2 describe the density functions for image intensities arising from the surface or the gap between the spheres, respectively. The dashed curve, labelled "J", is the joint intensity distribution function for the pebbled texture and an overhead illuminant.

function is 0.46 and its variance (on $logI$) is about $3x$.

6.0 The Derived Lightness Scale

We now have obtained image-intensity density functions for the three major factors that cause intensity variations in an image: reflectance, surface orientation and illumination, and surface roughness. Missing are intensity variations due to sources: specularities, the sun, the sky and cast shadows (other than those due to surface texture). The distribution of these variables is difficult to estimate but is expected to be small as compared with the three previous factors. For example, the 2 deg sun occupies only 1/7000th of the total sky and can be considered a singular intense point. More relevant intensity variations are the cloud patterns and North-South hemispheric variations in the sky. However, even these amount to only about 30% on the average (Wysecki and Stiles, 1967). It is this value which will be taken as a token estimate for source variations.

Table I summarizes the expected means and variances for the major factors that create intensity variations in an image. We now are in a position to calculate a joint probability density function for all these factors by successive convolution of their individual distributions (equations 7. 8, 9). The resultant probability density function is shown in Fig. 8. With source variations excluded, this density function has a mean of 0.025 and variance of $16x$. The resultant lightness scale is the integral of this function, as shown by the broken line.

TABLE I

FACTOR	MEAN I*	VARIANCE (on LogI)
Reflectance	0.1 - 0.2	10x
Surface Orientation and Illumination	.4	3x
Texture	.46	3x
Sources	.8	2x
TOTAL	0.020	18x

Figure T1. Table I. Summary of the expected means and variances of the separate major factors that create intensity variations in an image.

7.0 Relation to Empirical Photometric Scales

To determine whether the preceding analysis captures the major factors that contribute to the image-intensity distribution function, it is necessary to compare the derived probability function with empirical measurements. Two kinds of photometric data are of interest in this regard. The first is a comparison with the distribution of photometric measurements made by Jones and Condit (1949) for a large number of scenes. The second explores the relation between the derived lightness scale and the

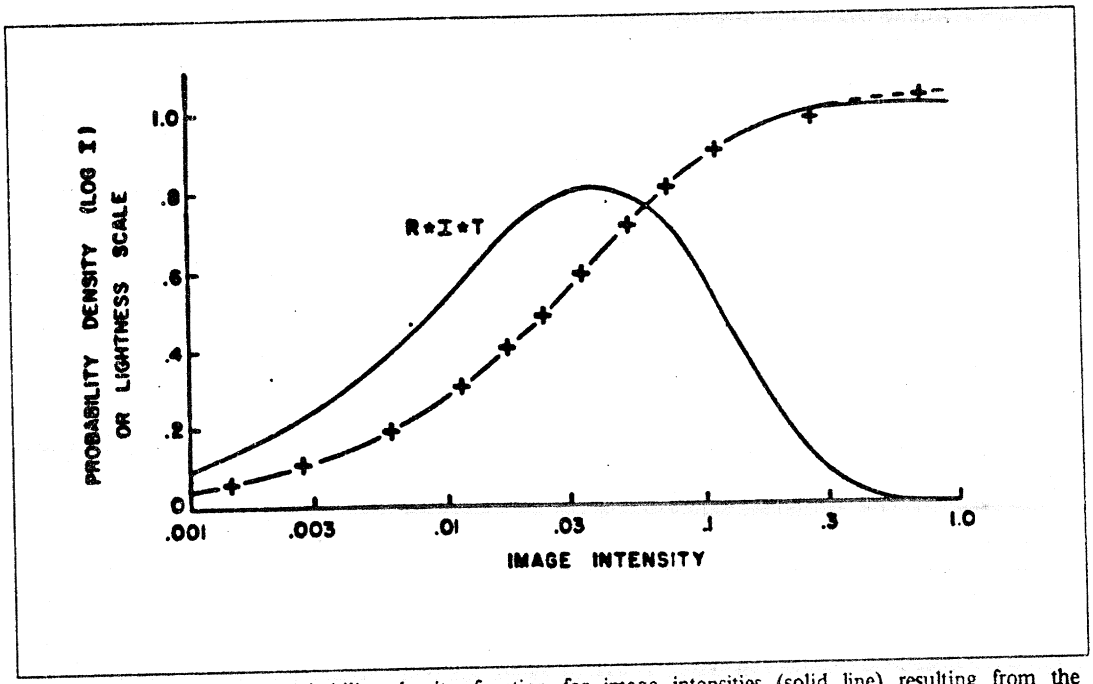

Figure 8. Threc-factor probability density function for image intensities (solid line) resulting from the convolution of intensity variations introduced by reflectance, surface orientation and surface roughness (texture). The ogive is the integral of this function, and is the theoretical lightness scale. The pluses describe the Naka-Rushton neural transfer function.

Munsell Scale.

7.1 The Jones and Condit Measurements

In the 1940's, Jones and Condit of Eastman Kodak (1949) obtained data on the luminances and luminance scales of 121 outdoor scenes. The luminance scale was defined as the ratio of the maximum to the minimum luminance. The luminances were measured with a portable, telescope-type visual photometer with a small field of view. The values of luminances found in different regions of one typical outdoor scene is shown in Table II. Note that the range of the measurements is almost 200 to 1.

Figure 9 is a plot of the distribution of the range of luminances found in the 121 scenes studied. The mean range is $160x$, with some values as high as 700 to 1. To estimate the range expected from the theoretical three-factor distribution of intensities, we must recognize that Jones and Condit were attempting to measure a practical maximum for the intensity range in scenes typically photographed. Their choice of scenes, and the measurements taken on each scene are therefore not random. Nevertheless, one constraint on their selection was that all scenes yielded at least a 30 to 1 luminance range, since this is the lowest range measured. Presumably the sky (or illuminant) was measured in each outdoor scene, and hence the greatest lower bound on the luminance measured was .033 ($=1/30$) relative to the maximum scene.

Returning to Figure 8, we then deduce that the remaining measurements were confined to the left portion of the image intensity distribution below the value .033. The mean of this portion of the

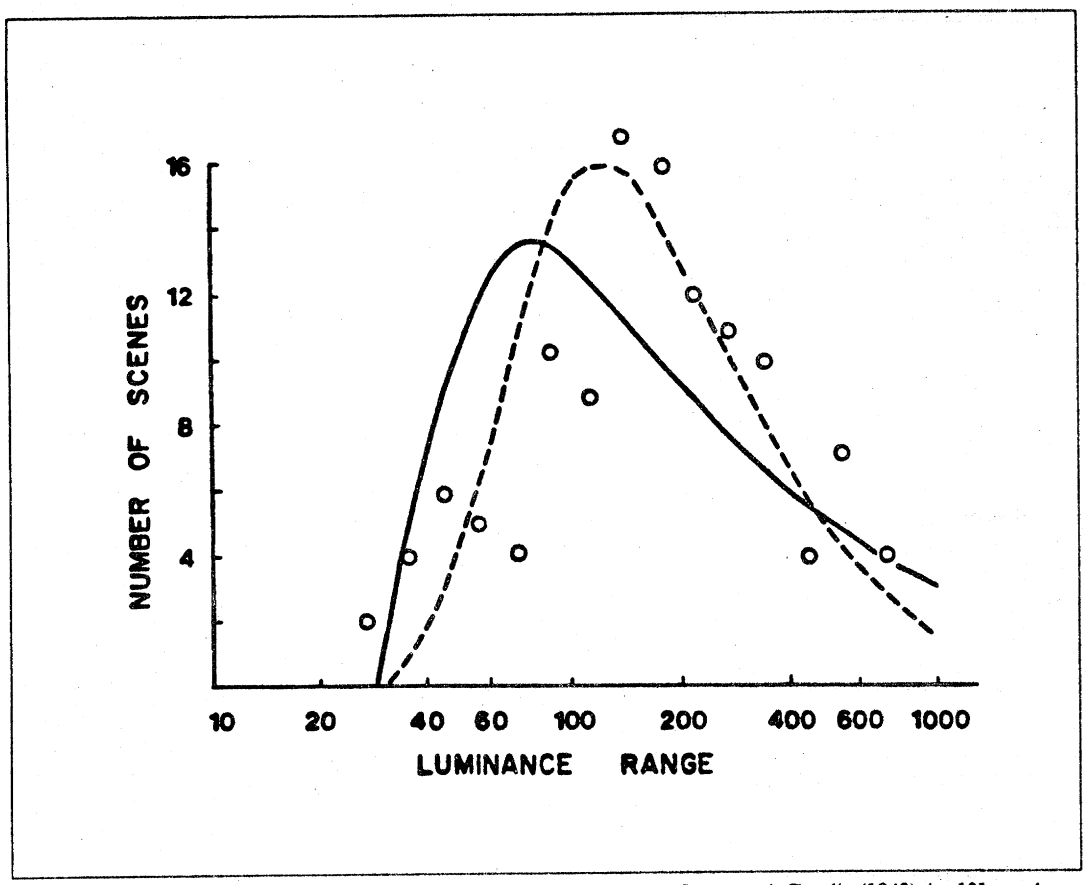

Figure 9. The distribution of the range of luminances found by Jones and Condit (1949) in 121 outdoor scenes is given by the open circles. The solid curve is a distribution of the range predicted from the theoretical distribution of image intensities. The dashed curve is the prediction based on the best log-normal approximation to the theoretical image intensity distribution.

distribution is 0.01, suggesting that the mean luminance range should be 100, as compared with the 160 value found by Jones and Condit. However, because Fig. 8 does not include source variations, our estimate of the mean is low by at least 20% (see Table I).

To recover the shape of the range distribution, we must consider the scene sampling procedure used by Jones and Condit. If the assumption is made that scenes with similar content will have similar probability distributions of image intensities, then the greatest changes in scene content will occur where the image intensity distribution changes most rapidly. Thus, if Jones and Condit chose a wide variety of scenes of different content, then the derivative of the image intensity distribution below .033 should yield the distribution of the luminance range. This derivative is shown as the solid line in Figure 9 and clearly is skewed to the left of the sample points.

If source variance is added to the theoretical intensity distribution of Figure 8, then the expected distribution of the luminance range is the dashed curve of Fig. 9. This is a quite reasonable match to the Jones and Condit data, considering estimation errors involved.

TABLE II

LUMINANCE VALUES IN AN OUTDOOR SCENE[3]

Area No.	Description of Area	Luminance in ft-L.
1	White cloud	3500
2	Blue sky	1350
3	Grass	1000
4	Side of stone bridge in sun	800
5	Water in sun	460
6	Stone bridge in open shade	300
7	Tree trunk (1)	135
8	Bridge in heavy shade	33
9	Tree trunk (2)	33
10	Heavily shaded portion of tree	18
LUMINANCE RANGE:		195

[3]From Jones and Condit (1949)

Figure T2. Table II.

7.2 The Munsell Scale

The Munsell Scale for lightness is one of several that characterize the relation between reflectance and the subjective brightness as seen by a "typical" human observer (Judd and Wysecki, 1975). Although the Munsell Scale is defined by a fifth order polynomial, good approximations can be found using rather simple formulae, especially considering the wide variations between the proposed scales. (For example, the original system by Priest, Gibson and McNicholas (1920) used a simple, square-root relation.) Undoubtedly, a rather simple relation could also be found to describe the integral of the complex convolutions required to construct the "ideal" lightness scale depicted in Fig. 8. Such a simple expression would give no insight, however, into the factors that underlie the scale and which give the scale its basic shape.

In the case of the Munsell Scale, the linking assumption is that the human visual system will optimize the spacing between reflectance samples seen under uniform illumination to match the expected distribution of reflectance in the world. If he does this, then the Munsell Scale should be very similar to the scale created by integrating the image-intensity distribution for reflectance, ρ. This is simply the integral of equation (7), which is plotted in Fig. 2 as the dotted loci labelled "K-M Theory". Qualitatively, the fit is good and within the range of proposed lightness scales. A near-perfect fit can be had by adding the effects of surface orientation (not shown).

8.0 Relation to Biological Transfer Functions

One important use of a lightness scale is to describe how image intensities should be transformed so that any one value is equally likely. Such a transformation thereby gives the most efficient sampling of the input. If the visual system is to code image intensity by neural firing levels, then the most effective transfer function should result in each level being equally likely (Laughlin, 1981). In this way, the amount of information per signal willl be maximized. The mapping of possible image intensities onto a range of neural activities is thus equivalent to defining an internal lightness scale. It should not be surprising, therefore, to find that the theoretically derived lightness scale is a good approximation to the neural transfer function.

The Naka-Rushton relation (Naka-Rushton, 1966) is one of the most widely-used neural transfer functions (Normann and Werblin, 1974; Hood, et al., 1979):

$$V/V^* = I^e/(I^e + \sigma^e) \tag{10}$$

where V is the retinal response relative to its saturation value V^*, I is the light intensity and σ and e are constants.

Figure 8 compares the three-factor lightness scale with the Naka-Rushton equation setting the exponent $e = 1$, $V^* = 12.5$ and a saturation constant $\sigma = 3$. The ogive is the theoretically derived curve that includes variations in image intensity due to surface orientation, texture and reflectance. The plusses, which are calculated from the Naka-Rushton relation (equation 10), fall close to the theoretical lightness scale function. A similar result has been noted by Laughlin (1981) in the con-

trast response function of first order interneurons of the insect compound eye. It appears, therefore, that the neural mechanisms that determine the visual transfer function are optimal for information processing.

REFERENCES

Bracewell, R.N., *The Fourier Transform and Its Applications*, McGraw-Hill, New York, 1978.

Brillouin, L., *Science and Information Theory*, Academic Press, New York, 1962.

Davidson, H. R. and Hemmendinger, H., "Color production using the two-constant turbid-media theory," *J. Opt. Soc. Am.* **56** (1966), 1102-1109.

Fechner, G.T., *Elemente der Psychophysik*, Bretkopf and Hartel, Leipzig, 1860.

Helmholtz, H. L. F., *Treatise on Physiological Optics*, trans. by J. P. Sonthall, Dover, New York, 1910.

Hood, D. C., Finkelstein, M. A. and Buckingham, E., "Psychophysical tests of models of the response function," *Vis. Res.* **19** (1979), 401-406.

Horn, B. K. P. and Sjoberg, R. W., "Calculating the reflectance map," *Applied Optics* **18** (1979), 1770-1779.

Jones, L. A. and Condit, H. R., *J. opt. Soc. Am. 39, pg. 94 (1949)*, and Chapter 22 by C. N. Nelson in Theory of Photographic Process, 3rd edition, Macmillan, New York, 1966.

Judd, D. B. and Wysecki, G., *Color in Business, Science and Industry*, Wiley, New York, 1975.

Keitz, H. A. T., *Light Calculations and Measurements*, St. Martins Press, New York, 1971.

Krinov, E. L., *Spectral reflectance properties of natural formations*, trans. by G. Belkov, NRC of Canada, Technical Tranlation 439, 1971.

Kubelka, P. and Munk, F., "Ein Beitrag zur Optik der Farbenstriche," *Z. tech. Physik.* **12** (1931), 593.

Land, E. H. and McCann, J. J., "Lightness and retinex theory," *J. Opt. Soc. Am.* **61** (1971), 1-11.

Laughlin, S., "A simple coding procedure enhances a neuron's information capacity," *Z. Naturforsch.* **36** (1981).

MacKay, D. M., "Psychophysics and perceived intensity," *Science* **139** (1963), 1213-1216.

Marr, D.C., *Vision: A Computational Investigation into the Human Representation and Processing of Visual Information*, W. H. Freeman & Co., San Francisco, 1982.

Naka, K. J. and Rushton, W. A. H., "S-potentials from colors within the retina of fish(cyprinidae)," *J. Physiol.* **185** (1966), 536-555.

Norman, R. A. and Werblin, F. S., "Control of retinal sensitivity," *J. Gen. Physiol.* **63** (1974), 37-61.

Priest, G., Gibson, K. S. and McNicholas, H. J., "An examination of the Munsell color system," *Natl. Bur. Std. Tech. Paper* **167** (1920).

Resnikoff, H. L., "On the Psychophysical Function," *J. Math. Biol.* **2** (1975), 265-276.

Richards, W., "Psycho-metrical numerology," *Tech. Engr. News* **XLVIII** (1967), 11-17.

Stevens, S., "To honor Fechner and repeal his law," *Science* **133** (1961), 80-86.

Torrance, K. E. and Sparrow, E. M., "Theory of off-specular reflection from roughened surfaces," *J. Opt. Soc. Am.* **57** (1967), 1105-1114.

Treisman, M., "A statistical decision model for sensory discrimination which predicts Weber's law and other sensory laws," *Percept. and Psychophys.* **1** (1966), 203-230.

van de Grind, W. A., Koederink, J. J., Landman, H. A. A. and Bouman, M. A., "The concepts of scaling and refractoriness in psychophysical theories of vision," *Kybernetik* **8** (1971), 105-122.

Wyszecki, G. and Stiles, W. S., *Color Science*, Wiley, New York, 1967.

Zipf, G. K., *Human Behavior and the Principal of Least Effort*, Addison-Wesley Press, Cambridge, 1949.

APPENDIX I

Derivation of Reflectance Density Function

Consider an opaque surface made up of fine particles of pigment embedded in a clear medium. As diffuse light strikes this surface, a portion of the flux will be reflected back, whereas another portion will pass into the layer either to be absorbed or to pass through. At the next deeper layer, again a portion of the light will be reflected back towards the surface and the remaining portion will be absorbed or transmitted through. For any arbitrary layer, there will be two factors that decrease the amount of light passing in to the next layer: absorption K and backward scatter S. These two coefficients are constants of the material comprising the surface.

The calculation of surface reflectance requires solving two differential equations for the net amount of light flux that leaves the surface. The general solution to this problem was first found by Kubelka and Munk in 1931. A special case of their solution is when the material itself is so thick that any further increases in thickness will not change the net flux leaving the surface. This condition is very suitable for most opaque natural objects and yields the following theoretical relations between absorption K, scatter S, and surface reflectance, ρ.

$$\rho = 1 + K/S - (K^2/S^2 + 2K/S)^{\frac{1}{2}} \tag{A1}$$

For an "ideal" achromatic material, its pigment will scatter no light, whereas its embedding medium or substrate will absorb no light (Judd and Wyszecki, 1965). Since the pigment has no scatter, its scatter coefficient is $S_P = 0$. Similarly, an ideal white substrate will absorb no light, hence its absorption coefficient $K_S = 0$. Thus, the pigment provides all the absorption K_P and the substrate is responsible for all the scatter, S_S. If the fraction of pigment in the mixture is C, then the net absorption coefficient in the mixture will be $C \cdot K_P$, and the scatter coefficient will be $(1 - C) \cdot S_S$. The value K/S for the mixture will then be:

$$K/S = C \cdot K_P/(1 - C) \cdot S_S \tag{A2}$$

Letting the two material constants K_P/S_S be represented by the single material constant, a, we have

$$K/S = Ca/(1 - C) \tag{A3}$$

Substitution into equation A1 yields text equation (4):

$$\rho = 1 + \frac{Ca}{(1-C)} - \frac{Ca}{(1-C)}\{1 + \frac{2(1-C)}{Ca}\}^{\frac{1}{2}} \tag{A4}$$

The final density function for reflectance ρ, then follows the derivation given in the text.

Since the density function (7) for reflectance has two free parameters, a and β, it is of interest to determine how sensitive this density function is to the choice of these values. To fit Krinov's

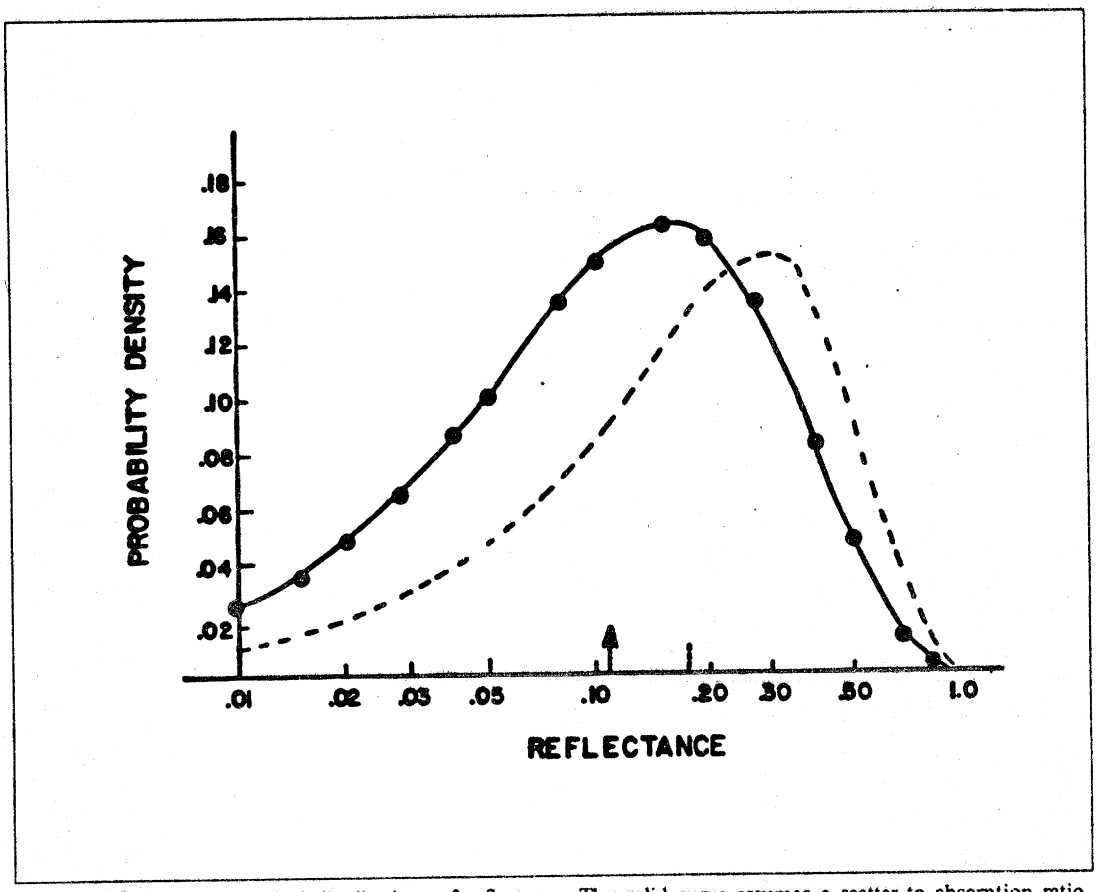

Figure A1. Two theoretical distributions of reflectance. The solid curve assumes a scatter to absorption ratio (α) of 0.5, and the same distribution as in text Fig. 3, but on a *logI* axis. The dashed curve assumes $\alpha = 1$. Although the two means are clearly different, the standard deviations are almost the same.

empirical distribution, α was chosen at $1/2$, which is in accord with values reported by Davidson and Hemmendinger (1966). However, the different materials can require quite different values. For example, a more appropriate α for paints would be 2, whereas for textiles, α is nearer $1/4$. Figure A1 shows two probability density functions for reflectance based on the Kubelka-Munk theory with $\alpha = 1/2$ (solid curve) and $\alpha = 1$ (dashed curve). Although the mean reflectance value changes from 0.12 to 0.18 for this change in α, the standard deviation of the reflectance distribution is altered hardly at all. This result is illustrated in Fig. A2, which shows how various choices of α and β affect the mean and standard deviation of the density function. Within the dotted rectangle, α ranges from $1/4$ to $1\frac{1}{2}$ and β ranges from $1/8$ to 1, but the standard deviation varies only from 2.7 to $4.3x$. Over 60%of the region, the standard deviation of the reflectance distribution is within 10%of $3.3x$. (In other words, 68%of the log reflectances lie within $1/3$ to 3.3 of the mean reflectance.) The measure of the variance of the distribution of reflectances was thus taken as $3.3^2 = 10$.

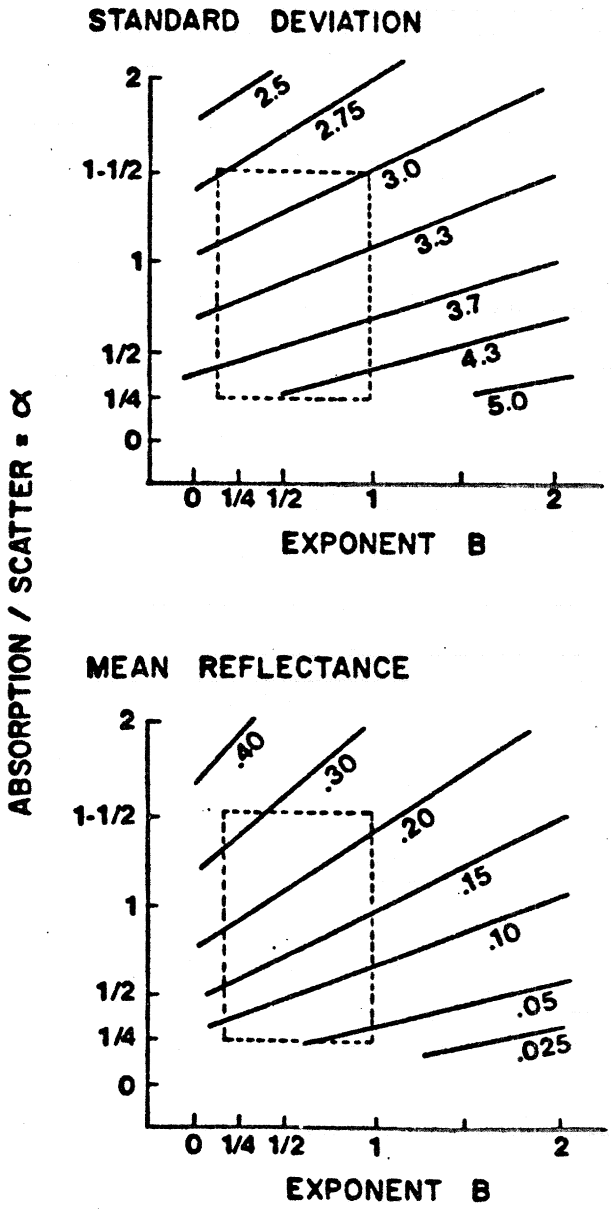

Figure A2. Effect of variations of the two parameters α, β on the mean and standard deviation of the probability density function of reflectances as derived from the Kubelka-Munk theory. The practical range of α and β is indicated by the dashed rectangle. Note that over this range, the standard deviation of the distribution does not change appreciably.

APPENDIX II

Derivation of Density Function for Surface Orientation and Illumination

AII. 1. Overhead Illumination Alone

Given the condition of an overhead point source and a spherical Lambertian surface viewed at 90° to the source direction (as shown in Fig. 4), the flux J_θ along any horizontal circle at angle θ to the illuminant direction **L** is given by

$$J_\theta = R \cdot F \cdot (\mathbf{N}_\theta \cdot \mathbf{L}) = R \cdot F \cdot cos\theta \tag{B1}$$

where **N** is the surface normal. To determine the flux $J_{\theta,\sigma}$ in the direction of the viewer, we find the projection of J_θ onto **V**:

$$J_{\theta,\sigma} = J_\theta \cdot (\mathbf{N} \cdot \mathbf{V}) = J_\theta cos\sigma \tag{B2}$$

The net image intensity $I_{\theta,\sigma}$ per unit area will then be $J_{\theta,\sigma}$ corrected for the foreshortening of the surface patch. This foreshortening will be proportional to $(\mathbf{N} \cdot \mathbf{V}) = cos\sigma$, yielding

$$I_{\theta,\sigma} = J_{\theta,\sigma}/cos\sigma = J_\theta$$

or from equation (B1)

$$I_{\theta,\sigma} = R \cdot F \cdot cos\theta = I_\theta \tag{B3}$$

The orthogonal (horizontal) circles about **L** thus correspond to loci of constant image intensity for Lambertian surfaces, regardless of the viewer's position.

To calculate the distribution of image intensities, we must now measure the area of the loci of constant I_θ, as projected onto the image plane. Imagine that each of the circles of constant I_θ is replaced by a ribbon or band of thickness ϵ. The projected width will then be less due to foreshortening, which is equal to $(\mathbf{N} \cdot \mathbf{V}) = cos\sigma$. For a sphere of unit radius, the total projected area of A_θ of a ribbon located at altitude Θ will thus be

$$A_\theta = \epsilon \cdot \int_{\phi=0}^{\pi/2} \pi \quad sin\theta \quad cos\sigma \quad d\phi \tag{B4}$$

where $\pi sin\theta$ is the arc length and $cos\sigma d\phi$ is proportional to the foreshortened area. (The angle ϕ is the angle between **N** and **V** as projected onto the horizontal plane—see inset to Figure 4.

Because $cos\sigma$ is a function of θ and ϕ, this relation must be determined before integration. For a unit vector $\mathbf{N} = 1$, the inset to Figure 4 shows that

$$cos\sigma = sin\theta \cdot cos\phi \tag{B5}$$

Substituting this relation into (B4) and performing the integration, we find that

$$A_\theta = \epsilon \cdot \pi \cdot sin^2\theta \tag{B6}$$

The area A_θ is thus proportional to the frequency of the image intensity along the locus where Θ is constant. But $sin\theta$ can be determined from equation (B3), remembering that $cos\theta = (\mathbf{N} \cdot \mathbf{L})$:

$$sin\theta = (1 - cos^2\theta)^{1/2} = [1 - (\frac{I_\theta^2}{RF})]^{1/2} \tag{B7}$$

Normalizing the image intensities to the maximum on the surface by multiplying all I_θ by $R \cdot F$, equations (B6) and (B7) can be combined to yield the following normalized probability distribution for image intensities:

$$pdf(I) = [1 - I^2] \tag{B8}$$

This simple expression thus describes the expected density function for image intensities of Lambertian surfaces due solely to direct overhead illumination. It is plotted as the solid line in the upper graph of Figure B1.

AII.2. Overhead Plus Extended Illumination

To calculate the image-intensity density function for a Lambertian sphere illuminated by a point source overhead plus an extended source, we must first determine the relative strength of the diffuse illumination. If this diffuse illumination arises solely from reflection off surrounding surfaces, then the density function of Fig. 3 (equation 7) provides a basis for estimating the diffuse light contribution relative to the original (point) source. This function (7) describes the probability of finding an object of reflectance ρ. To calculate the total of light reflected by all objects of reflectance ρ, we merely multiply the probability of finding ρ times ρ itself and sum over all ρ's:

$$T_{reflected} = \int_{\rho=0}^{1} pdf(\rho) \quad \rho \quad d\rho \tag{B9a}$$

Note that if all objects had a reflectance of 1, then the total incident light will be

$$T_{incident} = \int_{\rho=0}^{1} pdf(\rho) \cdot d\rho \tag{B9b}$$

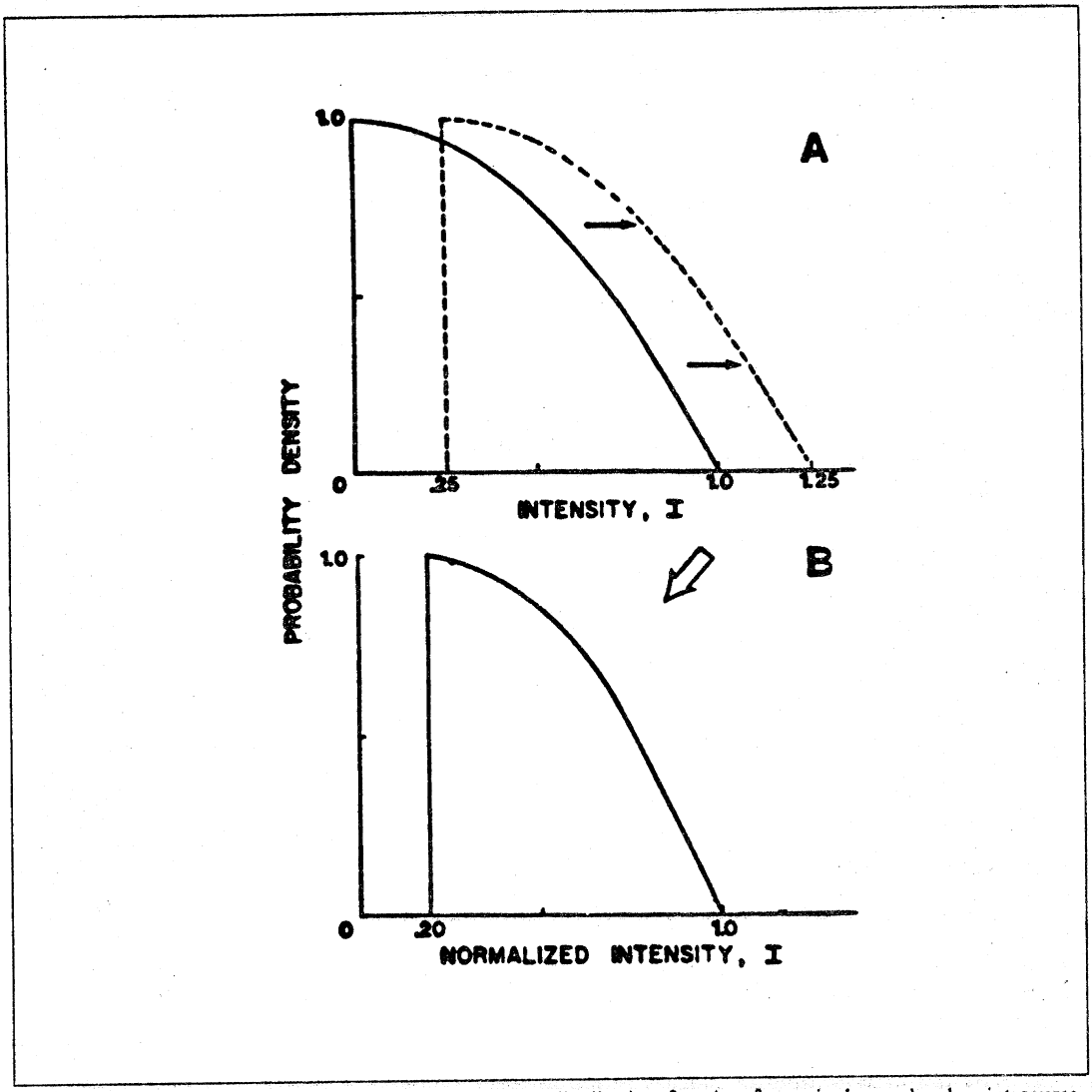

Figure B1. The upper solid line shows the intensity distribution function for a single overhead point source illuminating a uniform distribution of Lambertian surfaces. If extended illumination is also present, then the intensities are shifted to the right as indicated by the dashed line where 25% additional illumination everywhere is added as an example. When this new distribution is normalized so the maximum intensity is 1, the lower curve results, which is the expected image intensity distribution for an illuminant consisting of an overhead point source and plus an extended light source. These functions are also replotted in Fig. 5 on a $logI$ intensity axis.

The fraction of diffuse light relative to the strength of the direct light is thus $T_{reflected}/T_{incident}$. Numerical integration of text equation (7) yielded an estimate of 20% for the contribution of extended illumination to the total. (Note that this corresponds to the mid-point of the Munsell Scale.)

To visualize how extended illumination will modify the probability distribution of image intensities for a hemisphere of constant reflectance, refer to Fig. B1a. The solid curve describes $pdf(I)$ for overhead illumination alone. If an extended illumination of 25% of the source intensity ($I = 1$) is added everywhere to I, the new pdf will be shifted to the right as indicated. Renormalization of this curve so the maximum I is 1 will result in the new pdf described in Fig. B1b.

To quantify this result, let E be the fraction of the total source illumination due to extended sources, and I be the intensity due to the overhead source plus surface orientation, I_{max}. The combined illumination I' at any surface point will be

$$I' = E \cdot I_{max} + (1 - E)I \tag{B10}$$

To calculate the new probability density for I'; let I_{max} equal 1 to normalize I and then solve equation (B10) for I:

$$I = (I' - E \cdot 1)/(1 - E) \tag{B11}$$

Since $pdf(I)$ is known from equation (B8), substitution of (B11) yields

$$pdf(I') = 1 - (\frac{I' - E}{1 - E})^2 \tag{B12}$$

for $I' > E$, otherwise 0. Note that this density function is 1 at $I' = E$ and zero where $I' = 1$. To normalize the areas of $pdf(I')$ for different fractions of extended illumination, we may divide by $(1 - E)$ to give the following general equation for the intensity distribution resulting from extended and point overhead sources:

$$pdf(I) = \frac{1}{(1 - E)}[1 - (\frac{I - E}{1 - E})^2] \tag{B13}$$

for $I > E$, otherwise 0. Text Fig. 5 illustrates the form of this density function for no extended illumination ($E = 0$) and for 20% extended illumination.

APPENDIX III

Derivation of a Density Function for Texture

Two models for a textured surface are considered: one with the texture elements consisting of identical cylinders lying parallel on a flat surface of the same material, and illuminated from overhead, and the second texture created by closely packed spheres.

Although the utility of the "pebbled" surface model is emphasized in the text, it is simpler to derive its image-intensity density function by first considering the surface corrugated by cylinders. This approach has the further advantage of revealing the similarity between the density functions obtained from quite different model surfaces.

AIII.1 A "Matchstick" Surface

If cylindrical matches lie on a surface and are locally parallel, illuminated from above by a distant extended source such as the sky, then the significant variable is the cylinder separation measured in terms of the cylinder radius. The situation is depicted in Fig. C1, which is a cross-sectional view of a plane perpendicular to the cylinder axis.

The large hemisphere represents the overhead sky. The small circles are the ends of Lambertian cylinders, each of identical reflectance and size. Letting our coordinate axis begin at the center of the second circle, consider a point p on the cylinder located at a horizontal distance y from the top of the cylinder. Point p will be illuminated by the entire sky less that portion θ below its tangent plane, and less that second portion ϕ that is occluded by the adjacent cylinder. The intensity profile $I(y)$ along the cylinder will thus be:

$$I(y) = (\pi - \theta - \phi)/\pi$$

$$0 \leq y \leq 1 \tag{C1}$$

where

$$\theta = arc \quad sin(y) \tag{C1a}$$

$$\phi = arctan(1/B) - arctan[cos\theta/A] \tag{C1b}$$

where

$$A = S + 2 - y$$

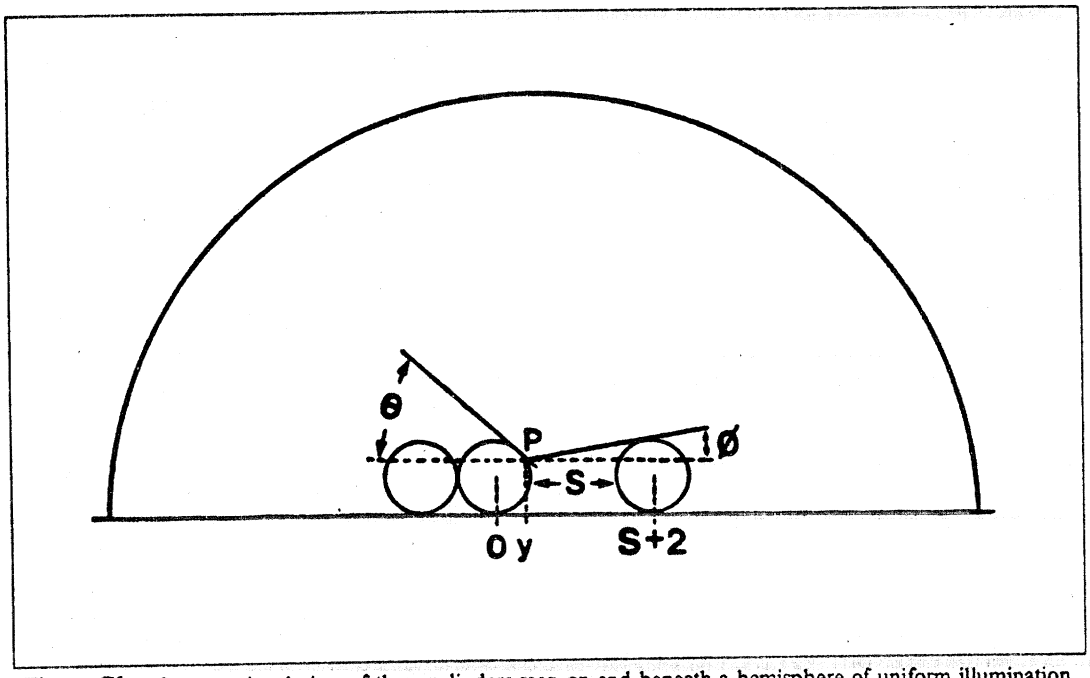

Figure C1. Cross-sectional view of three cylinders seen on end beneath a hemisphere of uniform illumination, such as the sky.

and

$$B = [A^2 + cos^2\theta - 1]^{1/2} \tag{C1c}$$

A similar geometric analysis yields the following relation for the illumination of any point lying on the ground planes in the gap between the cylinders:

$$I(y) = (\pi - 2arctan\frac{1}{A} - 2arctan\frac{1}{y})/\pi \tag{C2}$$

$$1 < y < (S+1)$$

where A is as before in (C1b). If the reflectance of the ground plane is not the same as that of the cylinders, we may calculate the image intensity profile for an overhead observer. Four such profiles are shown in Fig. C2 for cylinder separations of 0.5, 1, and 2 radius units.

. Two features are worth noting about these profiles. First, the intensity distribution along the cylinder surface is not affected appreciably by the neighboring cylinder, except at the edge. An excellent empirical approximation to this profile is the relation $I(y) = (1 - y^{3/2})^{1/2}$. Second, in the region of the gap between the cylinders, the intensity is rather constant, especially for separations less than twice the cylinder diameter. To a first approximation, this portion of the intensity profile can be described by the following relation, which is dependent only on the gap size S:

$$I(y) = 1 - (3/4)^s \tag{C3}$$

$$1 < y < (S+1)$$

These approximations will become useful in the case where the textured surface can be modelled by spherical pebbles lying on the ground plane.

To calculate the probability density function $pdf(I)$ for image intensities of a corrugated surface of cylinderical matchsticks, we now apply Bayes' rule as before:

$$pdf(I) = p(y) \cdot dy/dI \tag{C4}$$

where dy/dI can be determined by equations (C1) and (C2) or their approximations. Note that $p(y)$ will be constant because the sampling of image intensities will be at fixed increments in y for the orthographic view.

Fig. C2 shows how the density function varies for surfaces textured by cylinders spaced at intervals S. Note that the image intensity density function rapidly approaches a spike for cylinder separations greater than three times their radius. The greatest range in the intensity distribution occurs for $S = 0$, where the cylinders abut one another. Here the mean value is 0.8 and the variance is $1.2x$ (on a $logI$ scale).

AIII.2. A "Pebble" Surface

Consider next the case where the surface roughness can be approximated by identical spheres lying on a ground plane. As seen from above, the appearance in a small region may be depicted as in Fig. C3. Note that when the spheres abut one another, the triangular region ABC includes the entire intensity profile of the configuration because similar triangles will completely cover the surface. The approach will be to determine first the probability density function for the triangle ABC, and then to explore the effect of increased separation of the spheres upon this distribution.

Profile A: The intensity profile of A is determined by the angle of the tangent plane along A. This profile is at most that of two abutting cylinders whose axis is perpendicular to the plane of A. The cylinder profile is given in Fig. C2a, and is replotted in Fig. C4 as curve A. The actual profile along A will lie below that of C2a, because the tangent plane will intersect spheres F (and its counterpart F'). Although this reduction in the illumination can be estimated in principle, it is not important except near the juncture of the two spheres where the illumination is small. To a first approximation, therefore, the intensity profile of locus A will be that of Fig. C2a.

Profile C: Again, this profile will be estimated by making the cylinder approximation as before and ignoring the intersection of the tangent planes with the neighboring spheres. The upper bound on the profile C is thus that for a cylinder separation of $(3^{1/2} - 1) = 0.7$. This profile will be intermediate between that shown if Figs. C2b and c. The correct profile has been replotted in Fig. C4 for the locus C.

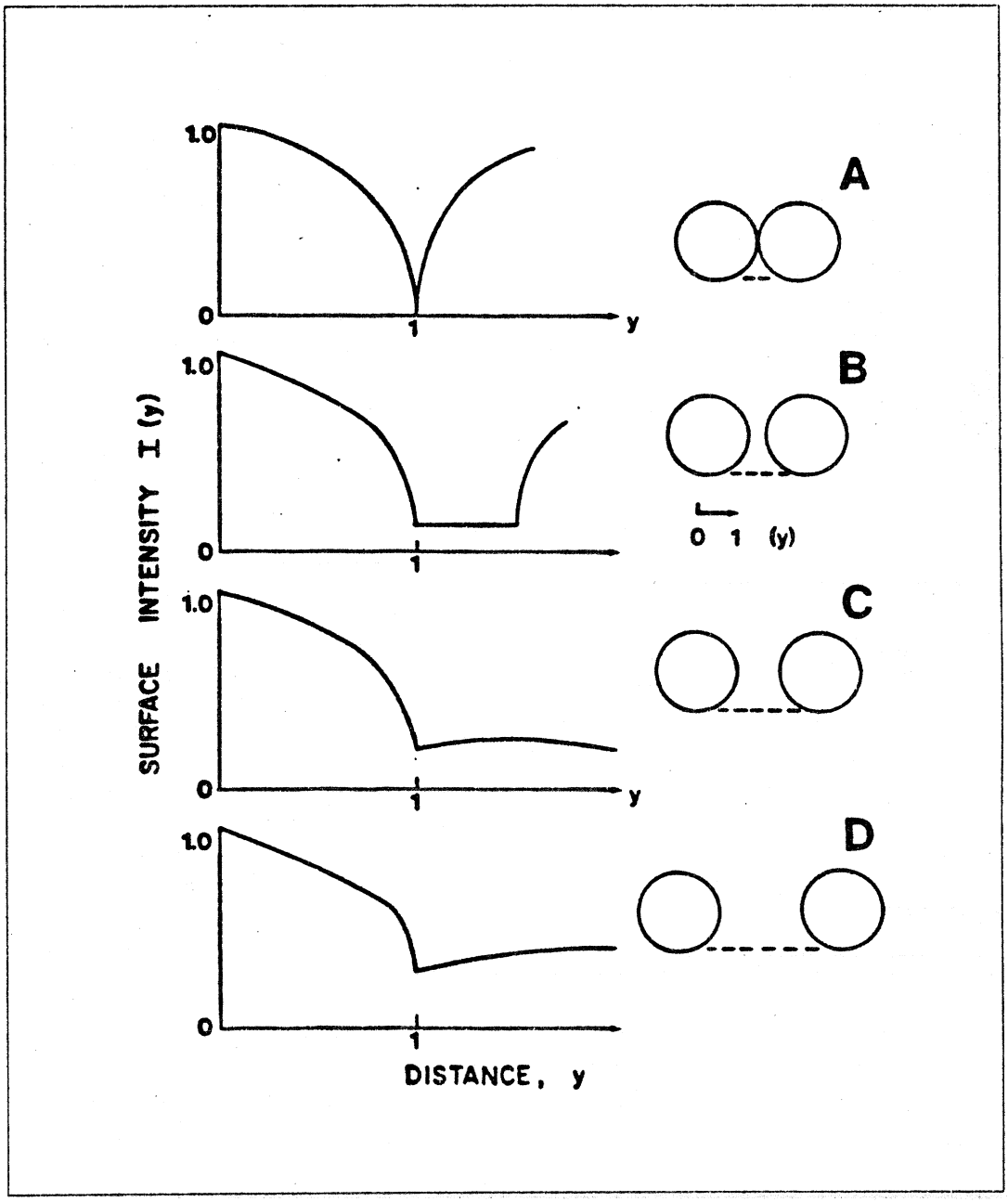

Figure C2. Intensity profiles along a surface comprised of cylinders. In A, the cylinders touch one another; in B the separation is 0.5 radius units; in C, 1.0 units and D, 2 radius units. Note that the profile along the cylinder surface is relatively independent of gap size.

Profile B: Recalling that in Fig. C2 the illumination in the gap between cylinders is essentially a function of gap width only, we can use this relation (C3) to estimate the profile of the gaps between adjacent spheres. Where locus B intersects A, the gap is zero, and so is the illumination, as shown in Fig. C4 at the unit distance $3^{1/2}$. As we proceed along the locus B toward C, the increase in gap size will increase the illumination of the ground plane to its maximal value at C located .13 units from the edge of the sphere. Again, this latter estimate is too high because the occlusion by spheres adjacent

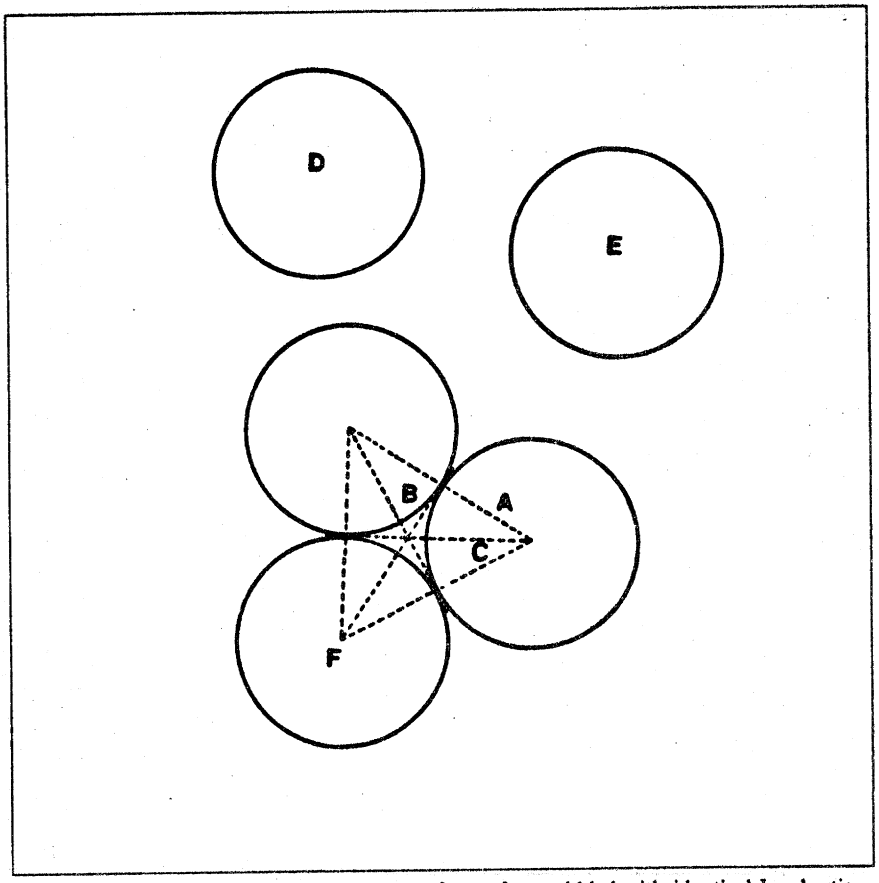

Figure C3. Overhead view of a portion of a surface pebbled with identical Lambertian spheres. The intensity profiles of the loci A, B and C as shown in Fig. C4.

to the tangent plane has not been taken into account. Nevertheless, it will serve as an estimate of the illumination profile along B.

The three profiles A, B, and C now describe the intensity profiles at the boundaries of the basic triangle that covers a "pebbly" surface of Lambertian spheres. To characterize the intensity at any point within this basic triangle, we note that in the sphere itself, the profile everywhere is essentially the same function of its radius, since the profiles A and C are very similar over the region 0 to 1. Using the approximating $I_S(y) = (1 - y^{3/2})^{1/2}$, we then find that the distribution of image intensities on the sphere will be:

$$pdf(I_S) = I^2(1 - I^2)^{1/3} \tag{C5}$$

if $p(I_S)$ is plotted on a $logI$ axis. Because the sphere itself occupies very close to 7/8ths of the area of the triangle to an overhead viewer, equation (C5) represents the major portion of the image intensity density function due to this type of roughness. (This function is plotted as the curve T_1 in Fig. 7.)

To determine the added effect of the dark gap between the spheres, we use the approximation for the gap illumination $I = (1 - .75^S)$ and note that the gap width, S is roughly proportional to the distance travelled along B from A to C. But since the gap width is proportional to the area of the gap

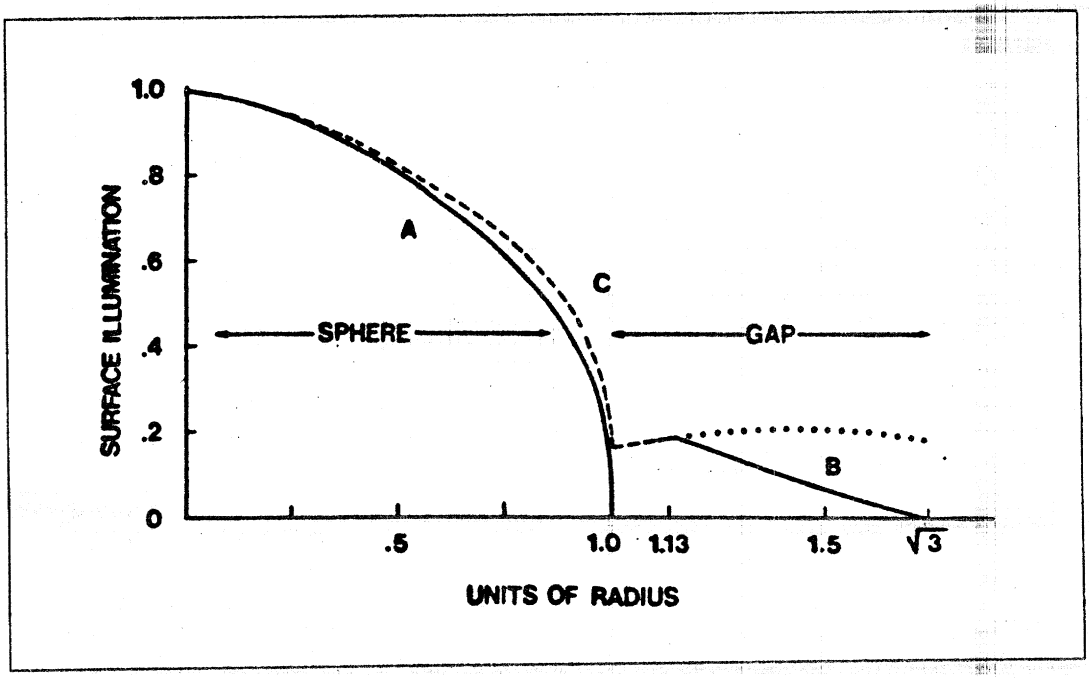

Figure C4. Three intensity profiles along the abutting spheres, as shown in Figure C3.

for a given fixed increment along B, we can find that the image intensity distribution function in the gap is roughly:

$$p(I_S) = \frac{I}{1-I} \cdot log\frac{1}{1-I}, \qquad 0 \leq I \leq .5 \tag{C6}$$

where a $logI$ axis is used. This distribution function is the lower lip on curve "T_2" in Fig. 7 having a weight of 1/8th, corresponding to the area of the gap relative to that sphere.

The total of curve "T" in Fig. 7 is thus the combined image intensity density function for both the gap and the sphere. (The same function is replotted on linear axes in Fig. 6b.) This envelope is thus an estimate of the intensity distribution that might be measured for a surface "pebbled" with roughly identical, closely-packed spheres. As the spheres move farther apart, the density function for intensity variations due to surface roughness must approach a spike at 1.0—i.e., the surface will be smooth and have a single intensity value everywhere. The upper curves in Fig. 6 give an indication of how fast a rough surface becomes smooth.

AIII.3. An Empirical Test

To insure that the image intensity density function for surface roughness shown in text Figs. 6 and 7 is an adequate model for a class of naturally textured scenes, a frontal photo of a leafy section of a rhododendron bush was taken and the image digitized. Fig. C5 shows the resulting intensity histograms as the irregular smooth curve, superimposed upon the "pebble" surface model which is

the dashed curve taken from Fig. 6b. Note that the characteristic "spike" due to the shadowed portions of the leaves is captured by the model. Considering the simplifying assumptions made in the derivation (as well as in the choice of scene!) the theoretical image intensity density function for textural variations can be considered adequate.

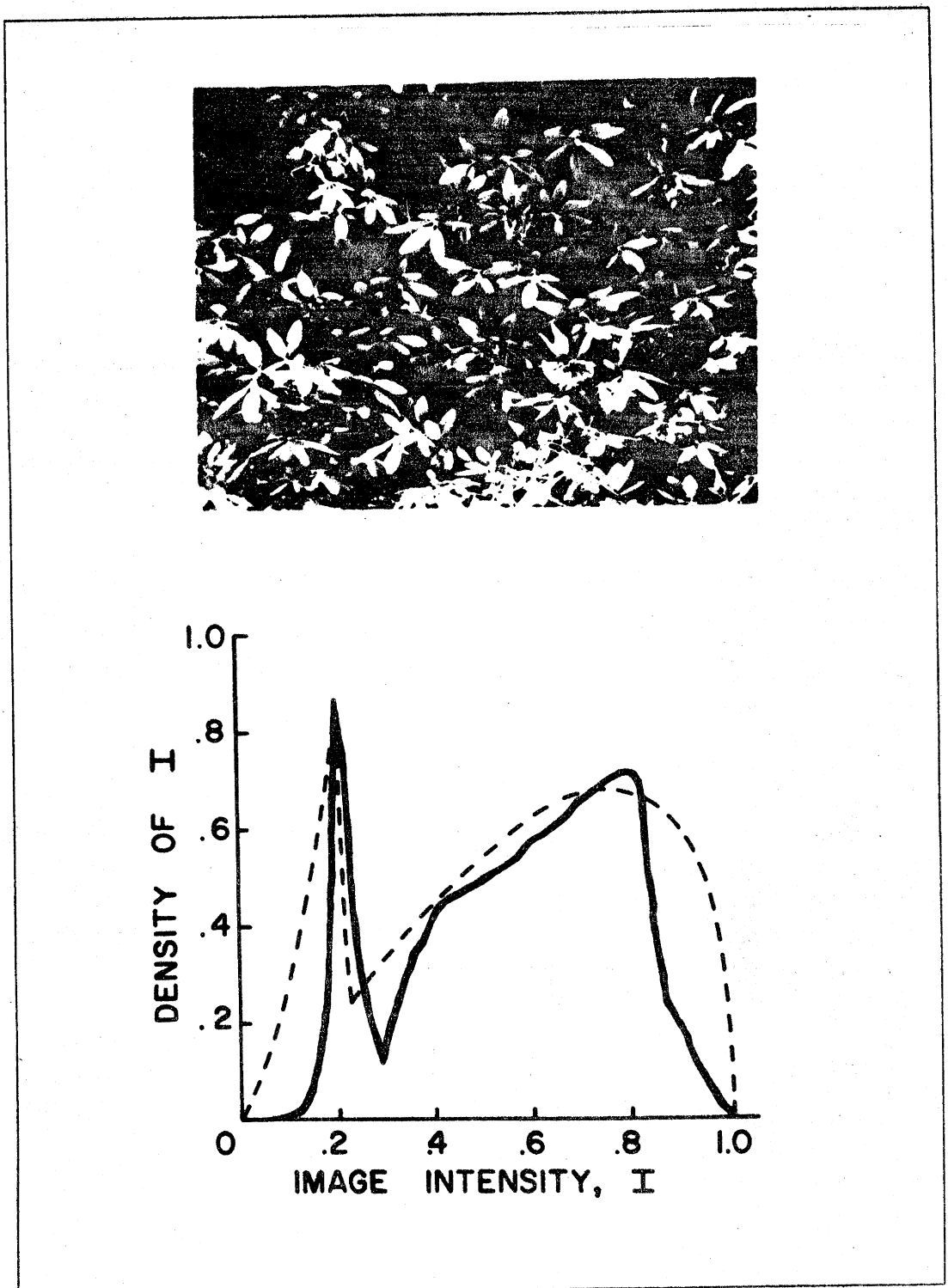

Figure C5. A comparison between an empirically measured image intensity distribution for a roughly textured surface and the "pebble" surface model. The smooth curve is the intensity histogram for the rhododendum bush shown in the top portion of the figure. The pebble-surface prediction is the dashed line taken from Fig. 6B (courtesy of D. D. Hoffman).